iScience

CellPress

Article

High-Throughput Small Molecule Screen Identifies Modulators of Mitochondrial Function in Neurons

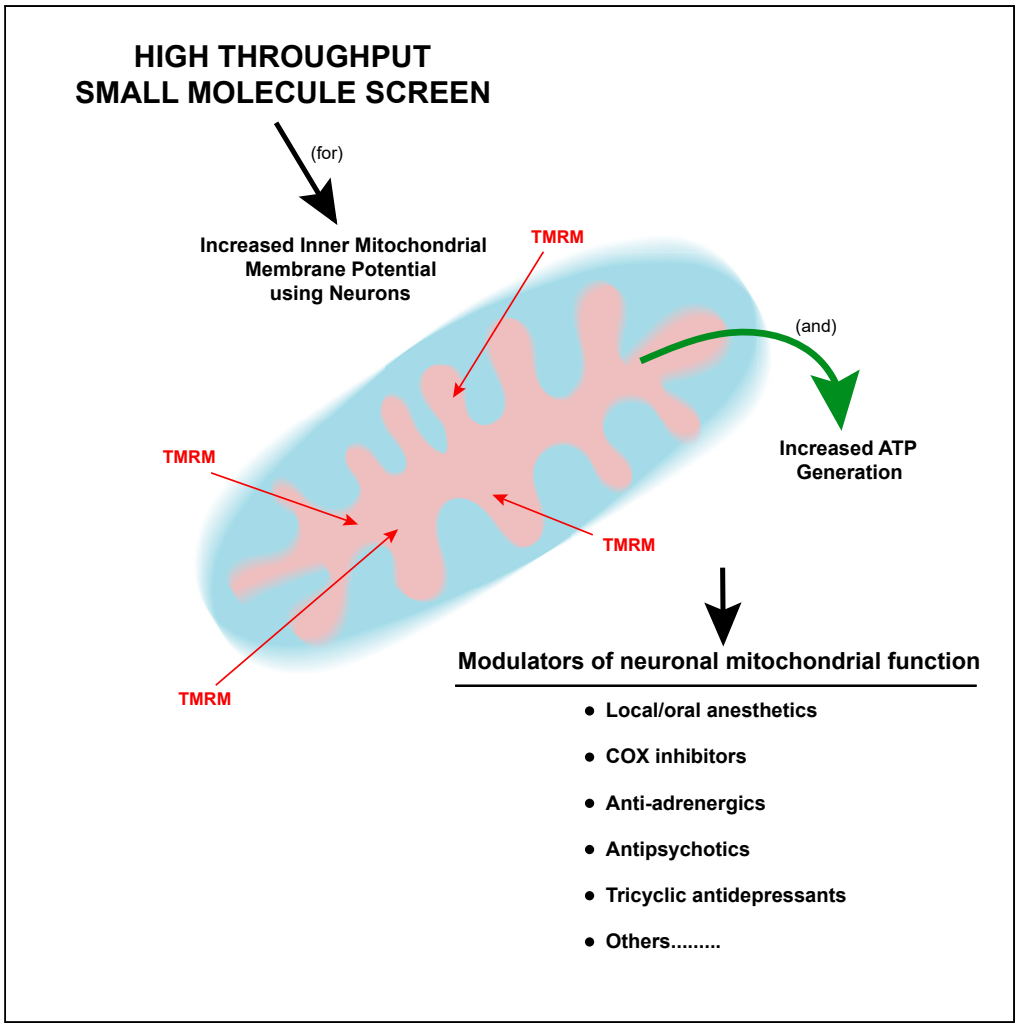

Boglarka H. Varkuti, Ze Liu, Miklos Kepiro, Rodrigo Pacifico, Yunchao Gai, Ted Kameneka, Ronald L. Davis

rdavis@scripps.edu

HIGHLIGHTS

Dozens of small molecules identified that enhance neuronal mitochondrial function

The small molecules promote mitochondrial health and enhance oxygen consumption

They protect neurons from toxic insults associated with neurodegenerative diseases

Varkuti et al., iScience *23*, 100931
March 27, 2020
https://doi.org/10.1016/j.isci.2020.100931

iScience

CellPress

Article

High-Throughput Small Molecule Screen Identifies Modulators of Mitochondrial Function in Neurons

Boglarka H. Varkuti,[1,3] Ze Liu,[1,3] Miklos Kepiro,[1,3] Rodrigo Pacifico,[1] Yunchao Gai,[1] Ted Kameneka,[2] and Ronald L. Davis[1,4,*]

SUMMARY

We developed a high-throughput assay for modulators of mitochondrial function in neurons measuring inner mitochondrial membrane potential ($\Delta\Psi_m$) and ATP production. The assay was used to screen a library of small molecules, which led to the identification of structural/functional classes of mitochondrial modulators such as local anesthetics, isoflavones, COXII inhibitors, adrenergic receptor blockers, and neurotransmitter system effectors. Our results show that some of the isolated compounds promote mitochondrial health, enhance oxygen consumption rate, and protect neurons against toxic insults found in the cellular environment of Alzheimer disease. These studies offer a set of compounds that may provide efficacy in protecting the mitochondrial system in neurodegenerative disorders.

INTRODUCTION

Mitochondrial function in neurons is critical for generating ATP (Brand and Nicholls, 2011; Vafai and Mootha, 2012), producing and detoxifying reactive oxygen species (ROS) (Zorov et al., 2014), buffering Ca^{2+}, mediating cell apoptosis, and synthesizing and releasing neurotransmitters (Duchen, 2000). Owing to these and other critical functions within high energy-demanding neurons, impairments in the mitochondrial system are associated very broadly with brain disorders (Connolly et al., 2018; Cai and Tammineni, 2016; Lezi and Swerdlow, 2012). These impairments include reduced mitochondrial numbers, membrane potential ($\Delta\Psi_m$), respiratory capacity, and ATP production, coupled with increased fragmentation and decreased synaptic function (Wang et al., 2009; Cai and Tammineni, 2017; Perez Ortiz and Swerdlow, 2019). Enhancing the function of neuronal mitochondria with small molecule therapeutics may offer effective treatment for these diseases (Alam et al., 2015; Moreira et al., 2010). However, prior screens used to identify such potential therapeutics have employed established cell lines, yeast, or fibroblasts (Kitami et al., 2012; Mortibouys et al., 2013). Given the unique architecture and physiology of neurons and the established differences in mitochondria across cell types (Calvo et al., 2016), screens for neuronal mitotherapeutics are best performed in neurons themselves. Thus we have searched for chemical enhancers of neuronal mitochondrial function using mammalian primary neurons to conduct a high-throughput screen (HTS).

We report here the development of an assay and results from a small molecule screen using neurons cultured from mouse brain and measuring $\Delta\Psi_m$, which provides the driving force on ATP synthase. Secondary screens for ATP production were employed to funnel the initial set of molecules, which were then tested for their effects on mitochondrial respiration and aspects of mitochondrial dynamics, including mitochondrial length and circularity, the latter being a morphological measure of mitochondrial health. The final set of molecules were subsequently shown to protect mitochondrial function from the insults of increased oxidative stress and an Alzheimer-like cellular environment produced in a genetic mouse model of Alzheimer disease. Strikingly, several classes of molecules had efficacy across these assays, including local anesthetics, estrogen agonists, isoflavones, and tricyclic antidepressants. These molecules offer starting points to probe the intricacies of the neuronal mitochondrial system and for potential mitotherapeutics.

RESULTS

Primary Neuron Assays for Inner Mitochondrial Potential and ATP Generation

The inner mitochondrial membrane potential ($\Delta\Psi_m$) and proton gradient generated by proton pumps during oxidative phosphorylation (OXPHOS) provide the energy to drive ATP synthesis. $\Delta\Psi_m$ is widely

[1]Department of Neuroscience, Scripps Research Institute Florida, Jupiter, FL 33458, USA

[2]Department of Molecular Medicine, Scripps Research Institute Florida, Jupiter, FL 33458, USA

[3]These authors contributed equally

[4]Lead Contact

*Correspondence: rdavis@scripps.edu

https://doi.org/10.1016/j.isci.2020.100931

used to measure the functional status and integrity of mitochondria (Connolly et al., 2018; Perry et al., 2011; Zorova et al., 2018). Hyperpolarization of $\Delta\Psi_m$ is associated with higher energy demand, as found in differentiating neuroblasts (Voccoli and Colombaioni, 2009), dividing versus quiescent cells (Huang, 2002), and developmentally active cells (Daniele et al., 2017; Medina et al., 2002). Depolarization of $\Delta\Psi_m$ is associated with diseased cells, aging, apoptosis, and toxic insults (Lezi and Swerdlow, 2012; Nadanaciva et al., 2011; Nicholls, 2004; Wagner et al., 2008). We measured $\Delta\Psi_m$ and then ATP production in cultured neurons to identify chemicals that increase the functional output of mitochondria.

The fluorescent dye tetramethylrhodamine, methyl ester (TMRM) was used at non-quenching concentrations for measuring $\Delta\Psi_m$ because of its fast equilibration time, low nonspecific binding to the plasma membrane, and reduced toxicity compared with the alternatives of TMRE, Rh123, JC-1, and $DiOC_6$ (Figures 1A, S1A, and S1B) (Connolly et al., 2018; Perry et al., 2011). We performed multiple control experiments before and during our screen to validate, optimize, and provide quality control for the TMRM assay including (1) identifying quenching and non-quenching TMRM concentrations in primary neurons (Figures S1A and S1B) and selecting the non-quenching, 10 nM concentration of TMRM for further experiments; (2) establishing that the necessary wash steps did not alter the integrity of the delicate plated neurons and are required for accurate TMRM fluorescence readings (Figures S1C and S1D) and measuring TMRM fluorescence from neurons treated with positive, neutral, and negative compounds to show their distinct effects (Figure S1E); (3) measuring TMRM fluorescence across 384-well plates treated with DMSO vehicle alone to identify and adjust for well position effects (Figures S2A and S2B); (4) monitoring DMSO-treated wells during the screen to track variability between replicates and across the eight different source plates used for the screen (Figures S2C and S2D); and (5) developing appropriate statistical procedures for data normalization and hit selection (Figure S3). We further optimized a luciferase-based ATP assay as an orthogonal screen to help extract artifacts obtained from the TMRM screen and to monitor the relationship between $\Delta\Psi_m$ measured with TMRM and ATP concentration in primary cultured neurons (Figure S4).

For the primary screen, we incubated 13 days *in vitro* (DIV13) primary neurons with 10 nM TMRM for 90 min to reach equilibrium before pin-tooling compounds from the Spectrum Collection from MicroSource. This library contains 2,400 structurally diverse compounds, the majority of which are marketed drugs or compounds in clinical trials. All compounds were assayed in quadruplicate at 12.5 μM, and mitochondria-localized TMRM fluorescence (Figures 1A–1A″) was measured at 4 and 24 h to identify compounds that have acute or delayed effects on $\Delta\Psi_m$ (Figure 1B). We predicted that acute hits might be compounds that directly and rapidly target the electron transport chain to modulate the efficiency of OXPHOS, whereas compounds with a delayed effect might modulate gene expression or signaling pathways to enhance mitogenesis and/or OXPHOS activities. From the 2,400 tested compounds, 16 (0.6%) were selected as putative hits increasing TMRM fluorescence at 4 h and 135 compounds (5.6%) increasing TMRM fluorescence at 24 h. Eleven of the compounds exhibited significant effects at both 4 and 24 h (>3 *Z* scores for the inner wells, >2.5 *Z* scores for the outer wells, Figures 1C–1D″).

We rescreened all 4- and 24-h TMRM hits alongside 40 DMSO control wells and 134 TMRM-negative compounds randomly selected from the original screen in a blind manner. There was a correlation of compound effect size on 24-h TMRM fluorescence between the primary screen and rescreen ($R^2 = 0.63$, Figure 1E). Of the 135 compounds 120 were confirmed as hits enhancing TMRM fluorescence at 24 h (89%). Of these, 112 (93%; Table S1) proved positive using the orthogonal assay for ATP production, elevating ATP levels by ~15% (>3 *Z* scores) compared within within-plate DMSO controls (Figure 1F). Although the correlation of ATP and TMRM effect sizes was more modest ($R^2 = 0.46$), the putative hits significantly enhanced TMRM fluorescence and ATP production compared with non-hit compounds or DMSO-treated controls (Figure 1F). Only two of the 16 (13%) compounds that elevated TMRM fluorescence at 4 h increased ATP levels. To probe the relationship between TMRM signal and ATP production, we compared the correlation coefficient between the TMRM fluorescence of all rescreened compounds and ATP production at 4 and 24 h. We found a very weak correlation between these two parameters for 4 h of incubation ($R^2 = 0.16$, $p < 0.0001$, Figure S4C) and a modest correlation ($R^2 = 0.46$, $p < 0.0001$, Figure 1F) for 24 h, indicating a general trend between the measured whole-well TMRM signal and higher energetics of the neuronal population. We focused our subsequent studies on hits selected after a 24-h incubation with neurons given the stronger relationship between TMRM fluorescence and ATP generation. Using this incubation time, the results indicate that increased $\Delta\Psi_m$ is a good, inexpensive surrogate for detecting elevated levels of ATP within neurons.

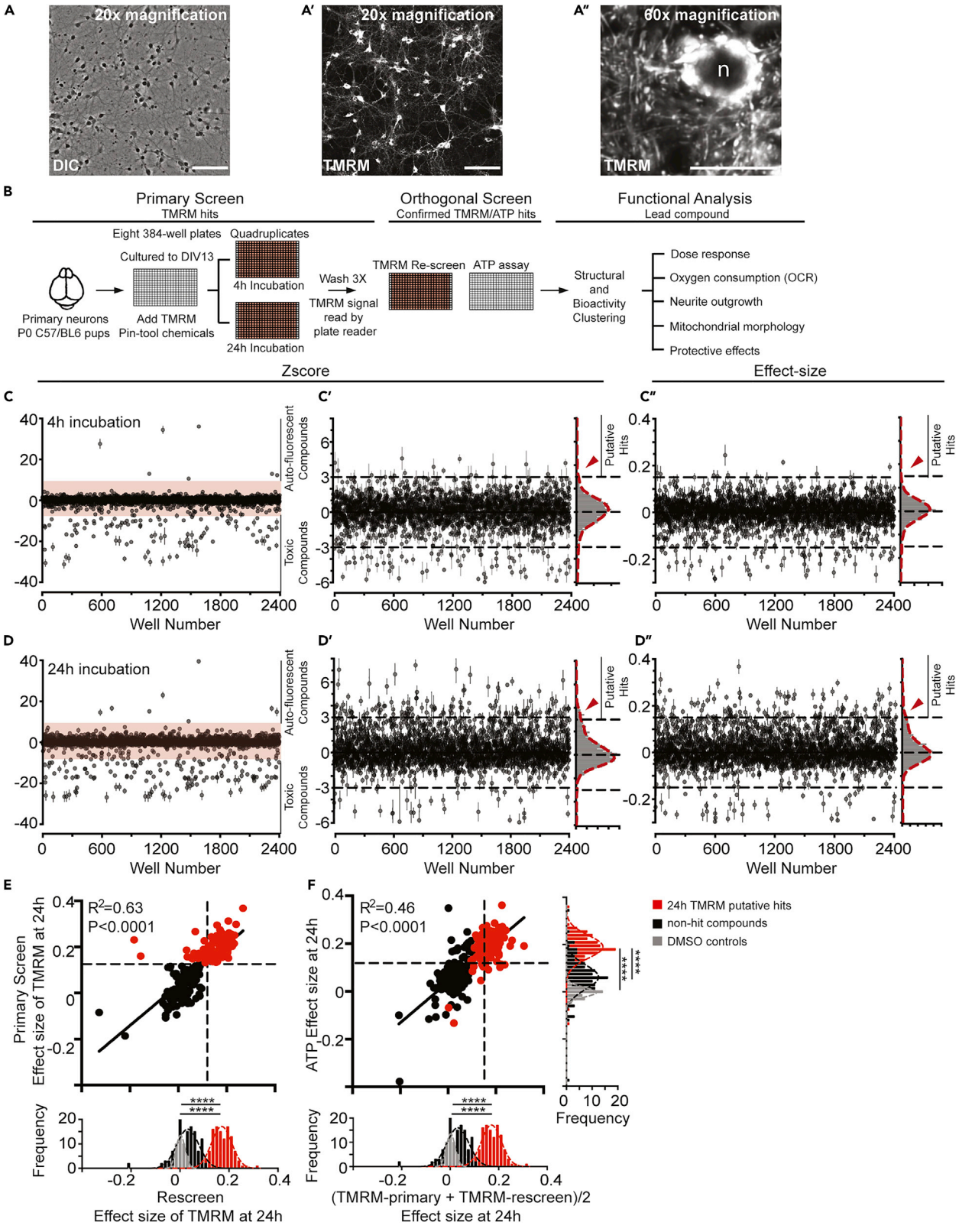
A
20x magnification
DIC
A′
20x magnification
TMRM
A″
60x magnification
n
TMRM
B
Primary Screen
TMRM hits
Orthogonal Screen
Confirmed TMRM/ATP hits
Functional Analysis
Lead compound
Eight 384-well plates
Quadruplicates
Cultured to DIV13
4h Incubation
24h Incubation
Primary neurons
P0 C57/BL6 pups
Add TMRM
Pin-tool chemicals
Wash 3X
TMRM signal
read by
plate reader
TMRM Re-screen
ATP assay
Structural
and
Bioactivity
Clustering
Dose response
Oxygen consumption (OCR)
Neurite outgrowth
Mitochondrial morphology
Protective effects
Zscore
Effect-size
C
4h incubation
C′
C″
D
24h incubation
D′
D″
Auto-fluorescent Compounds
Toxic Compounds
Putative Hits
Well Number
E
R2=0.63
P<0.0001
Primary Screen
Effect size of TMRM at 24h
Frequency
Rescreen
Effect size of TMRM at 24h
F
R2=0.46
P<0.0001
ATP Effect size at 24h
(TMRM-primary + TMRM-rescreen)/2
Effect size at 24h
****
24h TMRM putative hits
non-hit compounds
DMSO controls

Figure 1. TMRM and ATP Assays and Screens for Small Molecule Modulators of Neuronal Mitochondrial Function

(A–A″) Primary mouse cortical neurons loaded with TMRM and imaged 24 h later. The two leftmost images (20X) show the cell density at DIV14 (A) and fluorescent mitochondria in cell bodies and neurites (A′); the image (60X) at the right (A″) illustrates neuronal mitochondria at a higher power including the intense, perinuclear mitochondria. n = nucleus. Scale bar, 400 μm for (A and A′) and 20 μm for (A″).

(B) High-throughput screening pipeline for small molecule enhancers of neuronal mitochondrial function. **Primary screen:** Primary neurons were isolated, plated, and cultured to DIV13 and loaded with TMRM before compounds were added with a pin-tool. At 4 and 24 h after compound addition the neurons were washed and TMRM fluorescence was read. **Orthogonal screen:** TMRM hits selected from the primary screen were rescreened and tested for their ability to enhance neuronal ATP production in an orthogonal screen. **Functional analysis:** TMRM/ATP positive hits were clustered by structural similarity. Representative hits from main structural clusters were further assayed for dose response, effects on oxygen consumption (OCR), mitochondrial morphology, neurite sprouting, and protection to neurons against insults associated with neurodegenerative diseases.

(C–D″) (C and D) Scatterplots of normalized *Z* scores (Z) of TMRM fluorescence, (C′ and D′) as zoomed in (orange shading in C and D) to eliminate most toxic and autofluorescent reads, and (C″ and D″) effect size of TMRM signals at 4- (C–C″) and 24-h incubation (D–D″). *Z* score = $(value_{compound}-\mu_{plate})/\sigma_{plate}$. Effect size = $(value_{compound} - \mu_{plate})/\mu_{plate}$. *Z* score and effect size (E) values for each compound were calculated per plate using population statistics from four replicate plates. We used the population of "inactive" compound-treated wells as the control; see Figures S3A and S3B for details on the "non-DMSO-control" statistical approach. Results are plotted as means ± SEM from the quadruplicates. Putative hits that increased intracellular TMRM intensity above the plate mean (μ_{plate}) by 3σ for the inner wells and by 2.5σ for the outer wells were selected for rescreen. Distribution histograms of *Z* score and effect size are shown on the right side of (C′, C″, D′, and D″). Arrowheads indicate the subpopulation identified as putative hits.

(E and F) Orthogonal screen of putative TMRM hits measuring ATP production; 135 putative hits with effects at 24 h (red) from the primary screen were retested alongside 134 randomly selected non-hit compounds (black) and 40 DMSO controls (gray). The compound effect at 24-h incubation on TMRM fluorescence and ATP production was normalized to DMSO controls on the same plate in the rescreen. Data were calculated as $(value_{compound} - \mu_{DMSO})/\mu_{DMSO}$. The 135 putative 24-h hits (red) plus 134 non-hits (black) are shown in the plot. Each point represents the mean from four replicate wells. (E) Correlation plot of 24-h TMRM fluorescence from the primary screen and rescreen. Linear regression fitted to values generated from the plotted 269 compounds (black line, $R^2 = 0.63$). The distribution of normalized TMRM effect size in wells treated with putative hits (red), non-hits (black), and DMSO (gray) is shown along the abscissa. One-way ANOVA followed by Dunn's *post hoc* was used for comparisons with the DMSO control and non-hit groups. ****$p < 0.0001$. (F) Correlation plot of compound effects on ATP production and TMRM fluorescence. The distribution of compound effect size on TMRM fluorescence and ATP production after 24-h incubation is shown in the histograms across the abscissa and ordinate, respectively. The putative 24-h TMRM hits are labeled in red, non-hits in black, and DMSO-treated wells in gray. Linear regression fitted to values generated from the plotted 269 compounds (black line, $R^2 = 0.46$). One-way ANOVA followed by Dunn's post hoc was used for comparing with the DMSO control and non-hit groups. ****$p < 0.0001$. Compounds were selected as TMRM/ATP hits if the effect size for ATP generation was greater than 15% (>$3\sigma_{DMSO}$, dashed lines in E and F) in the orthogonal screen in addition to being confirmed as TMRM hits.

Structural and Functional Diversity and Potency of Modulators of Mitochondrial Function

We found that many of the confirmed 24-h TMRM/ATP hits were structurally related and grouped them using hierarchical clustering and Tanimoto similarities into several clusters (Figure 2). We also discovered that some of the structural clusters contain compounds with a similar therapeutic use (Figures 2 and S5–S7; Table S2). Surprisingly, nine of the hit compounds are topical/local anesthetics (primarily in Cluster 3, orange shading in Figure 2) that increase neuronal mitochondrial $\Delta\Psi_m$ and elevate ATP. Owing to this novel finding, we included representatives from this group in subsequent experiments (lidocaine, benoxinate, dyclonine). Although only two isoflavone compounds were identified (Cluster 4, green), genistein was reported by Ding et al. (2011) to increase $\Delta\Psi_m$ in primary cortical neurons treated with Aβ peptide. Therefore, we employed genistein in later experiments as a putative positive control compound. Cluster 4 also contains many steroid hormone receptor modulators and two COX inhibitors (gray). Estrogen derivatives were previously shown to contain neuro- and mitochondria-protective activity (Mortibouys et al., 2013, Sherman and Bang, 2018, Grimm et al., 2014, Irwin et al., 2008; Nilsen et al., 2007), but the mitochondrial effect of COX inhibitors was unexpected. Thus, we chose celecoxib for further characterization. Cluster 5 is composed of three indole alkaloids that have alpha-blocker activity (brown). One of them, yohimbine was previously found to be neuroprotective by inducing the NRF2-mediated antioxidant response (patent WO2012149478A3). Therefore, we included yohimbine in follow-up experiments as a potential positive control and to explore this activity further. Cluster 6 contains a collection of structurally similar alpha/beta-blockers for the treatment of high blood pressure and heart diseases (anti-adrenergics, brown), from which we chose carvedilol and naftopidil for further tests. We also highlight the interesting identification of several anti-psychotics and classic tricyclic antidepressants (pink), anti-cholinergics (purple), and anti-dopaminergic/anti-serotoninergic compounds (yellow) in Clusters 7 and 8, whose unanticipated functional modulation of mitochondria made them intriguing compounds for additional experiments. We added the antibiotic phenyl-aminosalicylate (Cluster 3, blue) and two well-known antiparkinsonian agents (Cluster 9, anti-cholinergic, purple) for some subsequent experiments to begin exploring how this rich set of structurally and functionally diverse compounds modulates the function of neuronal mitochondria.

Dose response assays (Figures S5–S7; Table S2) of selected compounds revealed that the EC_{50}'s for TMRM fluorescence and/or ATP enhancement were generally between 0.1 and 5 μM. Effect sizes were measured

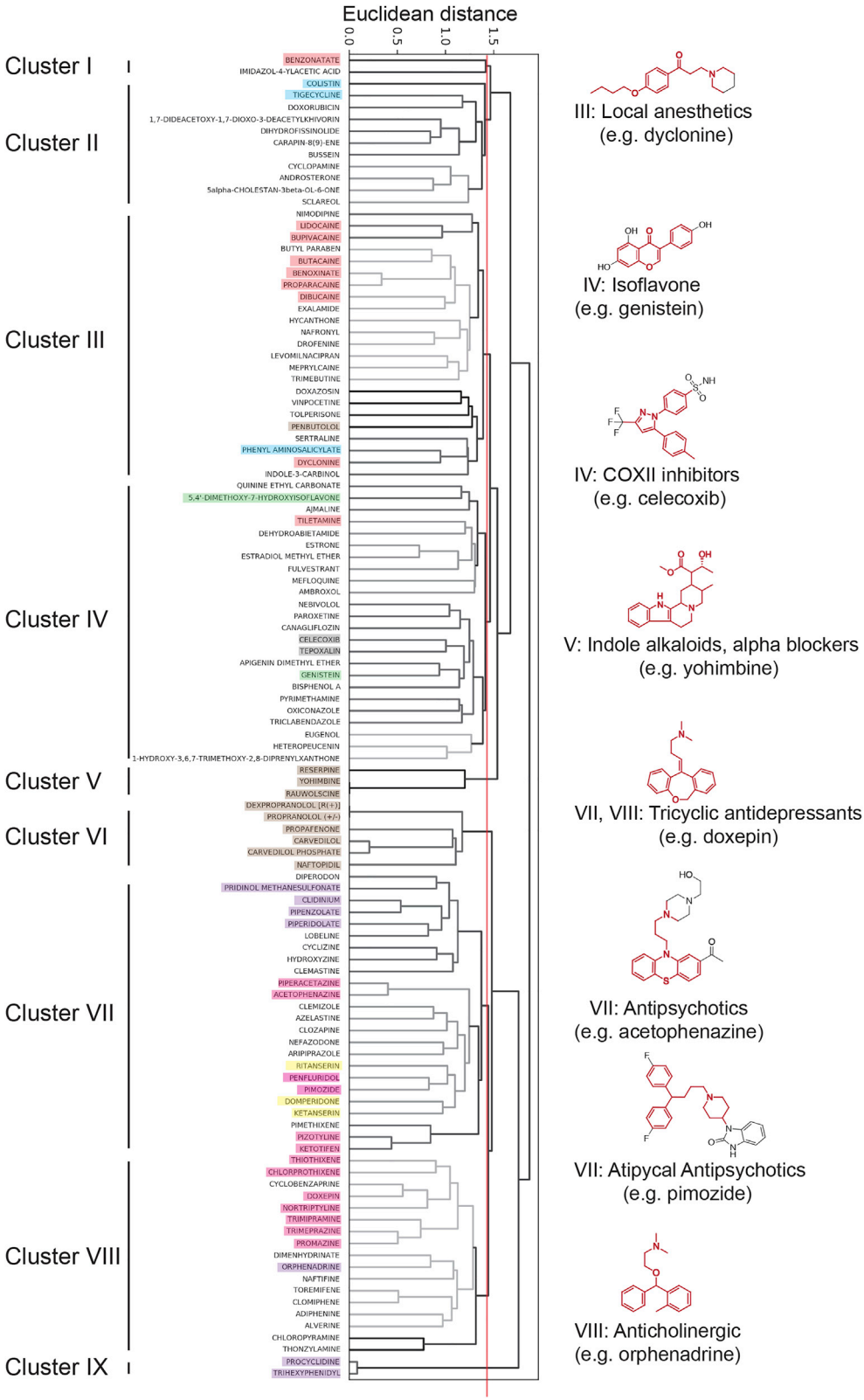
Euclidean distance
0.0
0.5
1.0
1.5
Cluster I
Cluster II
Cluster III
Cluster IV
Cluster V
Cluster VI
Cluster VII
Cluster VIII
Cluster IX
BENZONATATE
IMIDAZOL-4-YLACETIC ACID
COLISTIN
TIGECYCLINE
DOXORUBICIN
1,7-DIDEACETOXY-1,7-DIOXO-3-DEACETYLKHIVORIN
DIHYDROFISSINOLIDE
CARAPIN-8(9)-ENE
BUSSEIN
CYCLOPAMINE
ANDROSTERONE
5alpha-CHOLESTAN-3beta-OL-6-ONE
SCLAREOL
NIMODIPINE
LIDOCAINE
BUPIVACAINE
BUTYL PARABEN
BUTACAINE
BENOXINATE
PROPARACAINE
DIBUCAINE
EXALAMIDE
HYCANTHONE
NAFRONYL
DROFENINE
LEVOMILNACIPRAN
MEPRYLCAINE
TRIMEBUTINE
DOXAZOSIN
VINPOCETINE
TOLPERISONE
PENBUTOLOL
SERTRALINE
PHENYL AMINOSALICYLATE
DYCLONINE
INDOLE-3-CARBINOL
QUININE ETHYL CARBONATE
5,4'-DIMETHOXY-7-HYDROXYISOFLAVONE
AJMALINE
TILETAMINE
DEHYDROABIETAMIDE
ESTRONE
ESTRADIOL METHYL ETHER
FULVESTRANT
MEFLOQUINE
AMBROXOL
NEBIVOLOL
PAROXETINE
CANAGLIFLOZIN
CELECOXIB
TEPOXALIN
APIGENIN DIMETHYL ETHER
GENISTEIN
BISPHENOL A
PYRIMETHAMINE
OXICONAZOLE
TRICLABENDAZOLE
EUGENOL
HETEROPEUCENIN
1-HYDROXY-3,6,7-TRIMETHOXY-2,8-DIPRENYLXANTHONE
RESERPINE
YOHIMBINE
RAUWOLSCINE
DEXPROPRANOLOL [R(+)]
PROPRANOLOL (+/-)
PROPAFENONE
CARVEDILOL
CARVEDILOL PHOSPHATE
NAFTOPIDIL
DIPERODON
PRIDINOL METHANESULFONATE
CLIDINIUM
PIPENZOLATE
PIPERIDOLATE
LOBELINE
CYCLIZINE
HYDROXYZINE
CLEMASTINE
PIPERACETAZINE
ACETOPHENAZINE
CLEMIZOLE
AZELASTINE
CLOZAPINE
NEFAZODONE
ARIPIPRAZOLE
RITANSERIN
PENFLURIDOL
PIMOZIDE
DOMPERIDONE
KETANSERIN
PIMETHIXENE
PIZOTYLINE
KETOTIFEN
THIOTHIXENE
CHLORPROTHIXENE
CYCLOBENZAPRINE
DOXEPIN
NORTRIPTYLINE
TRIMIPRAMINE
TRIMEPRAZINE
PROMAZINE
DIMENHYDRINATE
ORPHENADRINE
NAFTIFINE
TOREMIFENE
CLOMIPHENE
ADIPHENINE
ALVERINE
CHLOROPYRAMINE
THONZYLAMINE
PROCYCLIDINE
TRIHEXYPHENIDYL
III: Local anesthetics
(e.g. dyclonine)
IV: Isoflavone
(e.g. genistein)
IV: COXII inhibitors
(e.g. celecoxib)
V: Indole alkaloids, alpha blockers
(e.g. yohimbine)
VII, VIII: Tricyclic antidepressants
(e.g. doxepin)
VII: Antipsychotics
(e.g. acetophenazine)
VII: Atipycal Antipsychotics
(e.g. pimozide)
VIII: Anticholinergic
(e.g. orphenadrine)

Figure 2. Hits from the Small Molecule Screen for Neuronal Modulators of Mitochondrial Function

Weighted Pair Group Method with Arithmetic Mean (WPGMA) clustering of the 112 confirmed TMRM/ATP 24-h hits into nine groups based on the Euclidean distance of Tanimoto similarities of their Morgan fingerprints with a cutoff at value 1.45 (red line). Representative chemical scaffolds for some clusters are highlighted in red. Shading: orange = local/topical anesthetics; green = isoflavones; gray = COX inhibitors; brown = alpha/beta blockers; pink = antipsychotics and tricyclic antidepressants; purple = anti-cholinergics; yellow = anti-dopaminergic/serotonergic compounds.

between 15% and 30%. Nearly all compounds, apart from yohimbine, exhibited inverted-U-shaped responses suggesting mitochondrial toxicity at high concentrations. Neurons are highly sensitive cells, and most compounds have detrimental effects at high concentrations.

Mitochondrial Functional Modulators Potentiate Respiration

The effects of the compounds on ATP generation suggested that they may increase mitochondrial respiration. To test this possibility, we selected yohimbine (indole alkaloid) and doxepin (tricyclic antidepressant) for the necessary and more complex, absolute oxygen consumption rate (OCR) experiments. OCR at baseline and in response to excess ADP/substrate (State3/3u) was measured and normalized to protein content (Salabei et al., 2014; Sims and Anderson, 2008) using primary neurons presented with compounds for 24 h. Primary neurons exposed to yohimbine or doxepin showed a weak, non-significant, but consistent trend toward an increased basal rate of respiration, potentially due to a modest increase in mitochondrial function and/or content (Figures 3A–3B′). More importantly, we observed a significant increase of State 3 and 3u respiration stimulated by either Complex I or Complex II substrates in mitochondria from cultured neurons treated with yohimbine (Figures 3A–3B′), and a significant increase with Complex I substrates for doxepin. We also took advantage of the water solubility of yohimbine to administer this compound to mice in drinking water across a period of 7 months. A similar respiratory increase was observed in mitochondria isolated from the whole brains of animals chronically treated with yohimbine (Figures 3C and 3D). We calculated the respiratory control ratios (RCRs, State $3/4_o$) to provide a broad index of mitochondrial function (Brand and Nicholls, 2011; Rogers et al., 2011). State 3 respiration measures the maximal ability of mitochondria for substrate oxidation and ATP generation. State 4_o, with OCR measured in response to oligomycin challenge, measures proton leak. The ratio between these states is influenced by most functions of OXPHOS, thus providing a net measure of the tightness between respiration and phosphorylation. Yohimbine treatment significantly increased RCR with both Complex I and II substrates with both mitochondria from cultured neurons and isolated brain mitochondria (Figures 3A′, 3B′, 3C′, and 3D′). Doxepin weakly increased RCR using Complex I, but not II, substrates in cultured neurons (Figures 3A′–3B′). Collectively, the enhanced State 3 respiration and RCR with yohimbine and the weaker effects of doxepin indicate more efficient substrate oxidation, electron transport, coupling to OXPHOS, and a lower proton leak, indicating a higher respiration capacity and efficiency in the treated mitochondria. Moreover, we previously reported that the anesthetic dyclonine produces beneficial effects in similar cell culture and *in vivo* experiments (Varkuti et al., 2020). Thus, representative compounds from three classes of functional mitochondrial modulators—indole alkaloids, tricyclic antidepressants, and local/topical anesthetics—all enhance neuronal mitochondrial function. These modulators may be acting directly on mitochondria or indirectly by stimulating cell signaling pathways that influence mitochondrial function (Sherman and Bang, 2018; Tsvetkov et al., 2010). However, the functional changes on mitochondria instilled by the tested compounds must be enduring and become independent of cytoplasmic signaling pathways, because increased function persists in permeabilized neurons and in mitochondria purified from cells.

Modulators of Neuronal Mitochondrial Function Alter Mitochondrial Morphology

To determine whether enhanced mitochondrial function is associated with mitochondrial morphological changes, we used a high-content assay developed in parallel to monitor aspects of mitochondrial dynamics in primary cultured neurons that conditionally express (Cre recombinase-dependent) mitochondrial-tagged GFP and cytosolic tdTomato reporters (Varkuti et al., 2020). We monitored two aspects of neuritic mitochondrial dynamics: the health of mitochondria as measured by the average circularity of axonal mitochondria, because defective mitochondria targeted for mitophagy become circular in shape, and the balance between fission/fusion measured by the average length of dendritic mitochondria. We also determined whether the compounds induced neurite sprouting by measuring the total area of neurites within the collected images (see Methods). Figure 4 illustrates the results of surveying a collection of functional modulators selected from five different structural clusters (Figure 2), quantified as robust *Z* scores relative to DMSO-treated control neurons. All the compounds tested showed a trend toward promoting

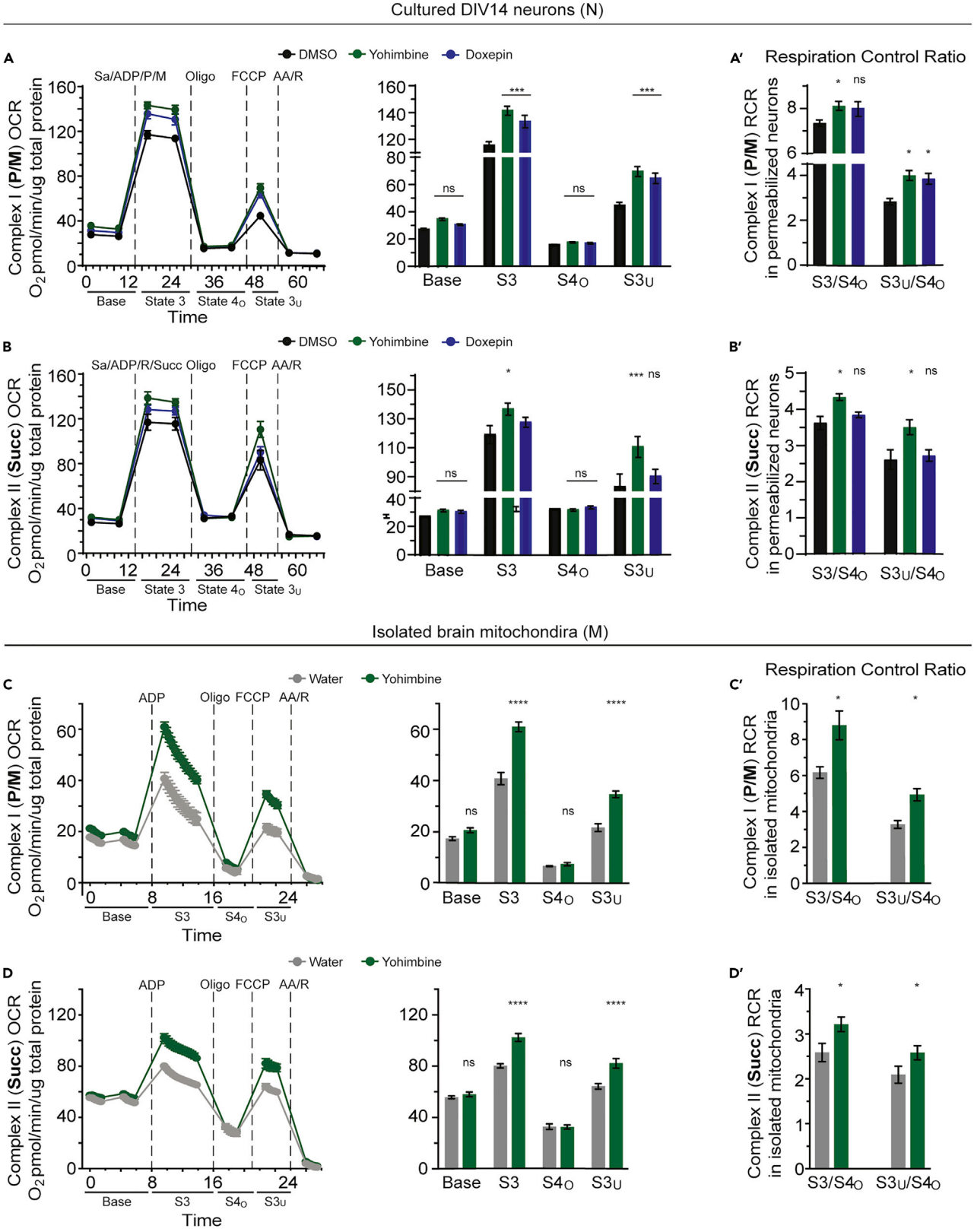
Cultured DIV14 neurons (N)
A
DMSO
Yohimbine
Doxepin
Sa/ADP/P/M
Oligo
FCCP
AA/R
Complex I (P/M) OCR
O2 pmol/min/ug total protein
Base
State 3
State 4O
State 3U
Time
A′
Respiration Control Ratio
Complex I (P/M) RCR
in permeabilized neurons
S3/S4O
S3U/S4O
B
Sa/ADP/R/Succ
Complex II (Succ) OCR
B′
Complex II (Succ) RCR
Isolated brain mitochondira (M)
C
Water
Yohimbine
ADP
C′
Complex I (P/M) RCR
in isolated mitochondria
D
Complex II (Succ) OCR
D′
Complex II (Succ) RCR

Figure 3. Effects of Compounds on Mitochondrial Function

(A–B′) Mitochondrial respiration in primary neurons exposed to compounds identified as mitochondrial functional enhancers from the screen. Before OCR measurements, DIV13 neurons were treated for 24 h with DMSO (0.1%) or the compounds (10 μM). Neurons were gently permeabilized using 25 μg/mL saponin (Sa). OCR measured from permeabilized neurons was displayed in the "middle point" mode showing a single OCR rate for each measurement period. Two measurements were performed under each condition (Base = baseline respiration, S3 = ADP/substrate-stimulated State 3 respiration, $S4_o$ = oligomycin-induced State 4 respiration) except for $S3_u$ (the FCCP-stimulated uncoupled State 3 respiration), which consisted of only one measurement. The right bar graph in each panel compares the averaged OCR from the two measurements in each condition among the DMSO- and compound-treated groups. The statistics shown were generated using two-way repeated measure ANOVA with the single control and the experimental groups. Sa = saponin, ADP = adenosine diphosphate, P = pyruvate, M = malate, Succ = succinate, Oligo = oligomycin, FCCP = carbonyl cyanide-*p*-trifluoromethoxyphenylhydrazone, AA = antimycin, R = rotenone. Note: We recently reported the experimental results for dyclonine (Varkuti et al., 2020), performed in parallel with yohimbine and doxepin as reported here. Thus the DMSO data shown are replicated from Varkuti et al. (2020). Statistical significance data were obtained from the DMSO control and all three experimental groups (yohimbine, doxepin, dyclonine).

(C–D′) Respiration of mitochondria isolated from brain neurons. Brain mitochondria were isolated from C57BL/6J animals administered either compound-supplemented (5 mg/kg yohimbine) or standard water for 7 months starting at 2 months of age. State 3 respiration was stimulated by addition of ADP (1 mM). Complex I substrates pyruvate and malate (P/M) or the Complex II substrate succinate (Succ) were preincluded in the assay buffer at 10 mM before the measurement of baseline respiration to maintain the healthy state of isolated mitochondria. OCR measured from isolated brain mitochondria is displayed in the "point-to-point mode" showing a series of OCR rates across each measurement period. The right bar graph in each panel compared the OCR value of the first measured point in each condition between the water- and compound-treated groups. Total protein was determined using the BCA assay (Bicinchoninic Assay) and used to normalize OCR into pmol O_2/min/μg total protein. Results in all panels are plotted as the mean ± SEM (n = 11–12). Data were analyzed by two-way repeated measure ANOVA followed by Bonferroni's multiple comparison tests. *$p < 0.05$, ***$p < 0.001$, ****$p < 0.0001$ compared with corresponding controls.

more oblong mitochondria after 24 h, and they exhibited significant potency (Z score < -2.0) compared with the control after 48 h of treatment. Notably, the identified mitochondrial OCR enhancers yohimbine, dyclonine, and doxepin exhibited robust effects. These results provide evidence that the functional modulators promote healthier mitochondria using the morphological surrogate of circularity.

The tested compounds also promoted the lengthening of dendritic mitochondria to Z scores ≥ 2.0 after 48 h of treatment. This observation is consistent with a report that mitochondrial fusion and fragmentation are associated with higher and lower $\Delta\Psi_m$ values, respectively, in neuroblasts and stable cell lines (Sherman and Bang, 2018; Voccoli and Colombaioni, 2009). Yohimbine, dyclonine, pimozide, and penfluridol were also observed to increase neuritic area after 48 h of treatment.

Neuronal Mitochondrial Modulators Provide Protection against Insults Associated with Neurodegenerative Disorders

Given the strong relationship between mitochondrial dysfunction and brain disorders, we tested a group of functional mitochondrial modulators for their potential to protect against two neurodegeneration-associated insults: neurons subjected to increased oxidative stress and those expressing Alzheimer-causing gene variants (neurons from 3XTG mice). Adding tert-butyl hydroperoxide to the cultures to increase oxidative stress severely reduced TMRM fluorescence at concentrations above 50 μM and led to complete cell death at concentrations >100 μM (Figure 5). Eight of the 10 compounds tested provided protection to the $\Delta\Psi_m$ from the toxic effects of increased oxidative stress (Figures 5A–5A″). Primary neurons isolated and cultured from 3XTG mice to DIV23 exhibited a ~20% reduction in TMRM fluorescence normalized to protein content per well when compared with C57Bl/6J neurons (Figures 5B–5B″). All compounds tested significantly increased $\Delta\Psi_m$ in the presence of the insult to the level observed for control B6 neurons (Figure 5B"). Remarkably, many of the compounds tested protect against both insults, including yohimbine, genistein, dyclonine, benoxinate, lidocaine, phenyl-4-amino salicylate, pimozide, and doxepin (Figures 5A″ and 5B″).

DISCUSSION

Our mitochondria-targeted TMRM/ATP high-throughput assay and screen using cultured primary neurons successfully identified multiple structural and functional clusters of compounds that enhance the function of neuronal mitochondria. The most surprising observation made concerns the large number and diversity of the compounds identified that potentiate mitochondrial function. Included among the modulators are the hormone derivatives yohimbine and genistein, which, consistent with published results, provided beneficial effects on mitochondrial function and overall neuronal health. These compounds stand out as positive controls for use in future HTSs that assay mitochondrial function. The most interesting and novel categories of hits include topical/local anesthetics as represented by dyclonine, classic tricyclic antidepressants as represented by doxepin, and the anti-psychotics as represented by pimozide and penfluridol. These results offer the prospect that molecules of these classes may offer protection against diseases that are associated with neuronal mitochondrial dysfunction. In addition, they

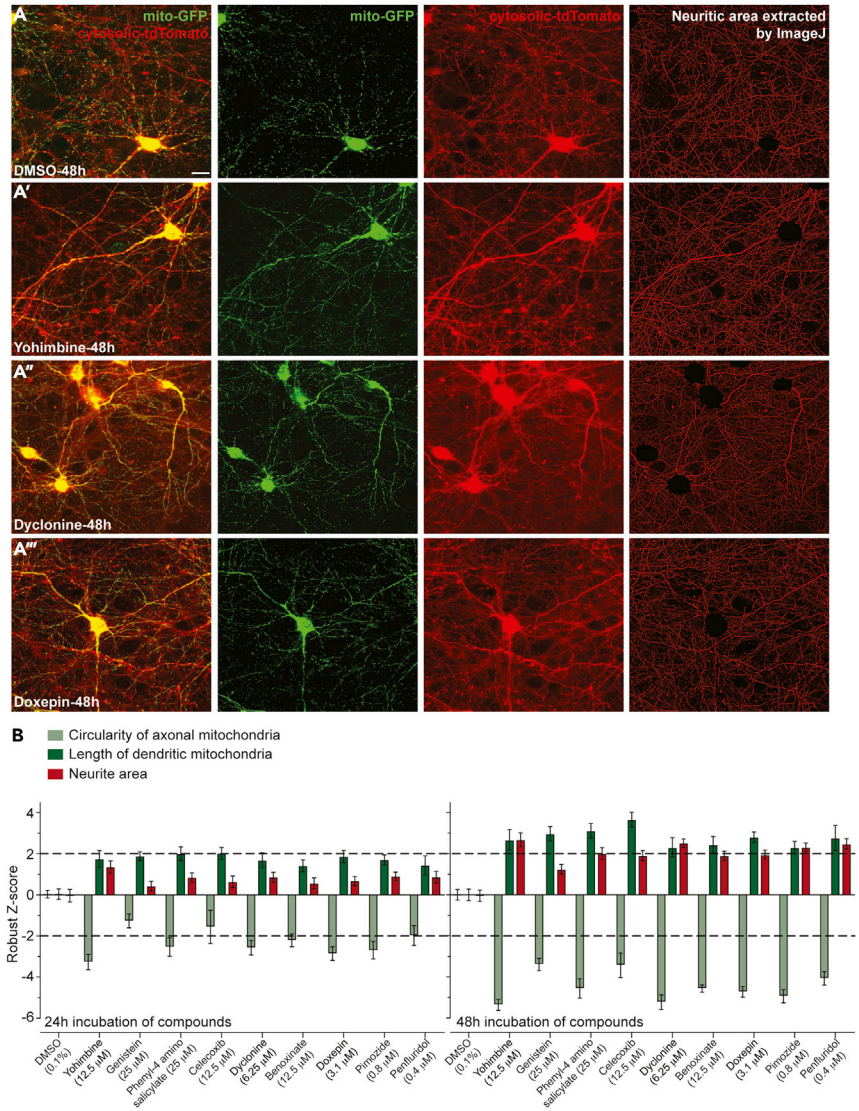

Figure 4. Effects of Compounds on Mitochondrial Morphology and Neurite Sprouting

(A–A‴ and B) Morphological changes in primary neuronal mitochondria due to treatment with mitochondrial functional modulators. (A-A‴) Using fluorescent reporters expressed in the mitochondria (mito-GFP, second column of images) and cytosol (cytosolic-tdTomato, third column of images), the circularity and length of mitochondria and the area of neurites in images were quantified after segmentation (e.g., extraction of neuritic area with ImageJ, fourth column of images). DIV13 neurons were treated with selected TMRM/ATP hit compounds or DMSO vehicle control and imaged after 24 or 48 h. Scale bar, 20 μm. (B) Neuritic mitochondria, which vary in length, were classed into axonal mitochondria (0.5 μm $\leq$ length $\leq$1.4 μm) and dendritic mitochondria (length $\geq$2.4 μm) based on our prior studies (Varkuti et al., 2020). The circularity of axonal mitochondria and the length of dendritic mitochondria were measured using the GFP signal and the neurite area from segmenting tdTomato fluorescence. These parameters were normalized as robust *Z* scores relative to in-plate, DMSO control wells. Data are presented as means ± SEM (n = 12 wells).

invite the speculation that the therapeutic effects of tricyclic antidepressants and anti-psychotics might include the functional modulation of brain mitochondria. On the technical side, our results show the feasibility of screening large libraries of compounds for effects on mitochondrial function directly in neurons, providing a more biologically relevant HTS platform for use in brain disease research.

Elucidating the mechanisms of action that these molecules have on the mitochondrial system in neurons is a long-term task, but prior studies offer a few intriguing possibilities. Estrogen derivatives (Cluster 4) and the

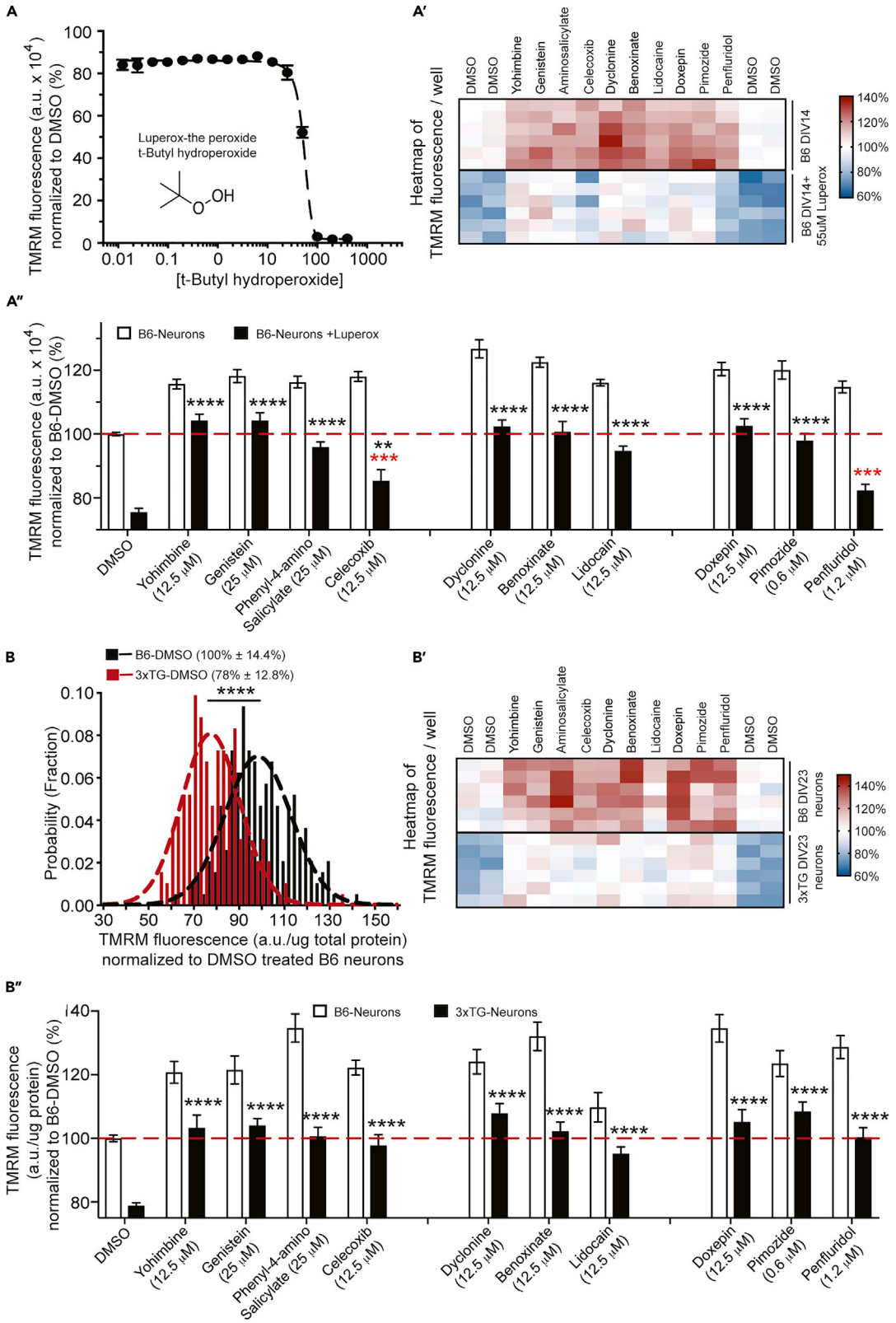
A
TMRM fluorescence (a.u. x 10^4) normalized to DMSO (%)
Luperox-the peroxide
t-Butyl hydroperoxide
[t-Butyl hydroperoxide]
A'
Heatmap of TMRM fluorescence / well
DMSO
Yohimbine
Genistein
Aminosalicylate
Celecoxib
Dyclonine
Benoxinate
Lidocaine
Doxepin
Pimozide
Penfluridol
B6 DIV14
B6 DIV14+ 55uM Luperox
140%
120%
100%
80%
60%
A''
TMRM fluorescence (a.u. x 10^4) normalized to B6-DMSO (%)
B6-Neurons
B6-Neurons +Luperox
Phenyl-4-amino Salicylate (25 μM)
B
B6-DMSO (100% ± 14.4%)
3xTG-DMSO (78% ± 12.8%)
Probability (Fraction)
TMRM fluorescence (a.u./ug total protein) normalized to DMSO treated B6 neurons
B'
B6 DIV23 neurons
3xTG DIV23 neurons
B''
TMRM fluorescence (a.u./ug protein) normalized to B6-DMSO (%)
3xTG-Neurons

Figure 5. Neuronal Mitochondrial Modulators Offer Protection against Insults Associated with Neurodegenerative Diseases

(A–A″) Mitochondrial modulators protect against the decline in $\Delta\Psi_m$ caused by increased oxidative stress. Primary forebrain neurons dissociated from C57BL/6J mice were plated into wells of four replicate, 384-well plates at the same density. At DIV13, TMRM was loaded at 10 nM along with 55 μM Luperox and a collection of mitochondrial modulators. Following 24-h treatment, the fluorescence was measured and normalized as %TMRM fluorescence relative to the within-plate DMSO controls. (A) The dose response effect of *t*-butyl hydrogen peroxide, a relatively stable peroxide used to increase oxidative stress in cultured neurons. DIV14 neuronal cultures in 384-well plates were treated with 16 different hydrogen peroxide concentrations from 10 nM to 400 μM, alongside paired DMSO controls, and whole-well TMRM fluorescence was assayed 24 h later. Points represent the mean ± SEM of three independent plates, each concentration tested in duplicate/plate; 24-h treatment with Luperox at 50 μM significantly reduced the whole-well TMRM fluorescence by ~40% in DIV14 neuronal cultures. Nearly complete cell death, shown as no intracellular TMRM accumulation, was observed in cells treated with Luperox at 100 μM or greater. (A′) Heatmap and summarized bar graph (A″) of TMRM fluorescence from untreated and hydrogen peroxide-treated neuronal cultures in response to DMSO (0.1%, control) and mitochondrial functional modulators from five structural clusters. The normalized TMRM fluorescence in the heatmap is the average per well across four replicates. Compounds that provided full neuroprotective effects are those that elevated the $\Delta\Psi_m$ depression observed in peroxide-challenged neurons to the level observed in neurons untreated with Luperox (red dashed line). Compounds at the concentration used that provided full protection to neurons included yohimbine, genistein, dyclonine, benoxinate, doxepin, and pimozide. Results are presented as mean ± SEM. n = 12 wells.

(B–B″) Mitochondrial modulators protect against the decline in $\Delta\Psi_m$ in primary neurons cultures made from 3XTG mice. Primary forebrain neurons dissociated from C57BL/6J (B6) and 3XTG mice were plated into wells of the upper and lower halves of four replicate 384-well plates at the same density. At DIV22, TMRM was loaded at 10 nM and the modulators were added. Following 24-h treatment, the well fluorescence was measured and normalized to total protein content to correct for potential differences in cell and/or neurite density between B6 and 3XTG neuronal cultures. (B) A significant reduction (~20%) in average normalized TMRM fluorescence was detected in the 3XTG cultures compared with the co-plated B6 neurons when treated only with 0.1% DMSO carrier. (B′) Heatmaps and summarized bar graphs (B″) of TMRM fluorescence from both B6 and 3XTG neuronal cultures in response to DMSO (0.1%, control) and the battery of mitochondrial functional modulators. The normalized TMRM fluorescence in the heatmap is the average per well across four replicates. All compounds provided full neuroprotective effects, indicated as those that elevated the $\Delta\Psi_m$ depression observed in 3TG neuronal cultures to the level observed in B6 neurons treated with DMSO (red dashed line). Results are presented as mean ± SEM (n = 24 wells). Data (A″ and B″) were analyzed by one-way ANOVA followed by Dunnett's multiple comparison tests. ***$p < 0.001$ (red), comparing drug-treated wells in the presence of the insult with control wells without the insult. **$p < 0.01$, ****$p < 0.0001$ (black), comparing drug-treated wells to control wells in the presence of the insult.

indole alkaloids (Cluster 5) have been reported to contain potent neuro- and mitochondrial-protective activity. This may occur through receptor-independent antioxidant activity, including the reduction of glutamate-induced lipid peroxidation and attenuation of endogenous and exogenous ROS, and/or by receptor-dependent (ERα, ERβ) anti-apoptotic activity, including the regulation of brain-derived neurotropic factor and the mitochondrial targeting of Bcl-2 and Bcl-xL, etc. (Klinge, 2008; Simpkins et al., 2008). Recently studies have revealed the extranuclear localization of estrogen receptors (ERα, ERβ) within mitochondria and the transport of exogenous estrogens into mitochondria (Chen et al., 2008; Psarra and Sekeris, 2008).

Given that the MicroSource Spectrum compound library consists of a large number of approved drugs, the mechanism of action for the hit compounds has already been explored in the context of the drug's original development. For instance, dyclonine and benoxinate are both local anesthetics that bind reversibly to activated sodium channels decreasing permeability and sensation. Doxepin as a tricyclic antidepressant is a known inhibitor of serotonin and norepinephrine uptake, also inhibiting histamine receptors to relieve local or generalized itching. The atypical anti-psychotic, pimozide, is a selective inhibitor of type 3 dopamine receptors thus decreasing dopaminergic transmission. It is possible, although unlikely, that these mechanisms of action perhaps funnel to some common effector of mitochondrial function and dynamics. However, given the diversity of the compounds identified along with a documented mechanism of action, we think it more likely that multiple known and unknown pathways exist that modulate the complexities of mitochondrial system dynamics and function.

A major future question prompted by this discussion is whether the mitochondrial modulators act directly on mitochondria to produce the observed effects or whether they work indirectly through various signaling systems. None of the data obtained so far address this important question, including the oxygen consumption experiments using mitochondria isolated from the brains of treated mice, because the modulators may have altered cellular signaling to instill long-term changes in mitochondrial function. One way to approach this unknown is to determine whether the modulators produce acute effects on the function of isolated mitochondria, assayed by either ATP generation or oxygen consumption experiments. The identification of distinct mitochondrial protein targets could be approached using photoaffinity-labeled mitochondrial modulators followed by proteomics experiments.

In summary, we have developed a high-throughput assay using primary neuronal cultures for mitochondrial function. Assay development using this cell type is critical for finding small molecule effectors of mitochondrial

function given the unique structure and physiology of neurons. A library screen identified a remarkably diverse set of compounds that modulate mitochondrial function that, in addition, alter the mitochondrial dynamic properties of circularity (health) and length and offer protection to the mitochondrial system against two insults associated with neurodegeneration: increased oxidative stress and the neuronal environment found in a mouse model for Alzheimer disease. This set of molecules offers a unique starting point for developing mitotherapeutics to protect the neuronal mitochondrial system from the toxicity associated with neurodegenerative disorders and to probe the intricacies of the mitochondrial system in neurons.

Limitations of the Study

The majority of this study utilized primary neurons from the mouse, which provide an imperfect model for neurons *in vivo*. Future studies will be directed toward *in vivo* efficacy of the compounds on the neuronal mitochondrial system. Although many of the compounds identified are known drugs with identified molecular targets, it remains unknown whether these same cellular targets are the ones that produce the observed effects on the mitochondrial system.

METHODS

All methods can be found in the accompanying Transparent Methods supplemental file.

SUPPLEMENTAL INFORMATION

Supplemental Information can be found online at https://doi.org/10.1016/j.isci.2020.100931.

ACKNOWLEDGMENTS

The research was supported by NIH grants 1R01MH109957 and 3R01MH109957-03S1 to R.L.D. Additional support was provided by a training grant in Alzheimer's Drug Discovery from the Lottie French Lewis Fund of the Community Foundation for Palm Beach and Martin Counties, the Coleman Hogan Fund for Memory Research, the Esther B. O'Keeffe Foundation, and major contributions from community philanthropists including W. Meyer, A. Dreyfoos, and P. McGraw.

AUTHOR CONTRIBUTIONS

Z.L. and R.L.D. conceptualized the project and designed most of the experiments. Z.L. developed the assays described; performed the screens, rescreens, and orthogonal screens; and performed cheminformatics and dose response, oxygen consumption, and experiments employing 3xTg neurons and increased oxidative stress. She was assisted by Y.G. R.P. treated mice with compounds and isolated the mitochondria. B.H.V. and M.K. developed and performed experiments employing high-content imaging. They also reanalyzed all the primary and orthogonal screening data. T.K. assisted with chemical and biological informatics. Z.L. and R.L.D. wrote the initial draft of the manuscript; B.H.V. and M.K. drafted revised versions of the manuscript. The final versions were edited and approved by all available authors.

DECLARATION OF INTERESTS

A US patent application related to some of the findings presented has been filed.

Received: March 20, 2019
Revised: January 16, 2020
Accepted: February 17, 2020
Published: March 27, 2020

REFERENCES

Alam, N.M., Mills, W.C., 4th, Wong, A.A., Douglas, R.M., Szeto, H.H., and Prusky, G.T. (2015). A mitochondrial therapeutic reverses visual decline in mouse models of diabetes. Dis. Model. Mech. *8*, 701–710.

Brand, M.D., and Nicholls, D.G. (2011). Assessing mitochondrial dysfunction in cells. Biochem. J. *435*, 297–312.

Cai, Q., and Tammineni, P. (2016). Alternations in mitochondrial quality control in Alzheimer's disease. Front. Cell. Neurosci. *10*, 24.

Cai, Q., and Tammineni, P. (2017). Mitochondrial aspects of synaptic dysfunction in Alzheimer's disease. J. Alzheimers Dis. *57*, 1087–1103.

Calvo, S.E., Clauser, K.R., and Mootha, V.K. (2016). MitoCarta2.0: an updated inventory of mammalian mitochondrial proteins. Nucleic Acids Res. *44*, D1251–D1257.

Chen, J.Q., Brown, T.R., and Yager, J.D. (2008). Mechanisms of hormone carcinogenesis: evolution of views, role of mitochondria. Adv. Exp. Med. Biol. *630*, 1–18.

Connolly, N.M.C., Theurey, P., Adam-Vizi, V., Bazan, N.G., Bernardi, P., Bolaños, J.P., Culmsee,

C., Dawson, V.L., Deshmukh, M., Duchen, M.R., et al. (2018). Guidelines on experimental methods to assess mitochondrial dysfunction in cellular models of neurodegenerative diseases. Cell Death Differ. *25*, 542–572.

Daniele, J.R., Esping, D.J., Garcia, G., Parsons, L.S., Arriaga, E.A., and Dillin, A. (2017). High-throughput characterization of region-specific mitochondrial function and morphology. Sci. Rep. *7*, 6749.

Ding, B., Yuan, L., Yu, H., Li, L., Ma, W., Bi, Y., Feng, J., and Xiao, R. (2011). Genistein and folic acid prevent oxidative injury induced by β-amyloid peptide. Basic Clin. Pharmacol. Toxicol. *108*, 333–340.

Duchen, M.R. (2000). Mitochondria and calcium: from cell signalling to cell death. J. Physiol. *529*, 57–68.

Grimm, A., Schmitt, K., Lang, U.E., Mensah-Nyagan, A.G., and Eckert, A. (2014). Improvement of neuronal bioenergetics by neurosteroids: implications for age-related neurodegenerative disorders. Biochim. Biophys. Acta *1842*, 2427–2438.

Huang, S.G. (2002). Development of a high throughput screening assay for mitochondrial membrane potential in living cells. J. Biomol. Screen. *7*, 383–389.

Irwin, R.W., Yao, J., Hamilton, R.T., Cadenas, E., Brinton, R.D., and Nilsen, J. (2008). Progesterone and estrogen regulate oxidative metabolism in brain mitochondria. Endocrinology *149*, 3167–3175.

Kitami, T., Logan, D.J., Negri, J., Hasaka, T., Tolliday, N.J., Carpenter, A.E., Spiegelman, B.M., and Mootha, V.K. (2012). A chemical screen probing the relationship between mitochondrial content and cell size. PLoS One *7*, e33755.

Klinge, C.M. (2008). Estrogenic control of mitochondrial function and biogenesis. J. Cell Biochem. *105*, 1342–1351.

Lezi, E., and Swerdlow, R.H. (2012). Mitochondria in neurodegeneration. Adv. Exp. Med. Biol. *942*, 269–286.

Medina, J.M., Lopez-Mediavilla, C., and Orfao, A. (2002). Flow cytometry of isolated mitochondria during development and under some pathological conditions. FEBS Lett. *510*, 127–132.

Moreira, P.I., Zhu, X., Wang, X., Lee, H.G., Nunomura, A., Petersen, R.B., Perry, G., and Smith, M.A. (2010). Mitochondria: a therapeutic target in neurodegeneration. Biochim. Biophys. Acta *1802*, 212–220.

Mortibouys, H., Aasly, J., and Bandmann, O. (2013). Ursocholanic acid rescues mitochondrial function in common forms of familial Parkinson's disease. Brain *136*, 3038–3050.

Nadanaciva, S., Murray, J., Wilson, C., Gebhard, D.F., and Will, Y. (2011). High-throughput assays for assessing mitochondrial dysfunction caused by compounds that impair mtDNA- encoded protein levels in eukaryotic cells. Curr. Protoc. Toxicol., Chapter 3, Unit 3. 11.

Nicholls, D.G. (2004). Mitochondrial membrane potential and aging. Aging Cell *3*, 35–40.

Nilsen, J., Irwin, R.W., Gallaher, T.K., and Brinton, R.D. (2007). Estradiol in vivo regulation of brain mitochondrial proteome. J. Neurosci. *27*, 14069–14077.

Perez Ortiz, J.M., and Swerdlow, R.H. (2019). Mitochondrial dysfunction in Alzheimer's disease: role in pathogenesis and novel therapeutic opportunities. Br. J. Pharmacol. https://doi.org/10.1111/bph.14585.

Perry, S.W., Norman, J.P., Barbieri, J., Brown, E.B., and Gelbard, H.A. (2011). Mitochondrial membrane potential probes and the proton gradient: a practical usage guide. Biotechniques *50*, 98–115.

Psarra, A.M., and Sekeris, C.E. (2008). Steroid and thyroid hormone receptors in mitochondria. IUBMB Life *60*, 210–223.

Rogers, G.W., Brand, M.D., Petrosyan, S., Ashok, D., Elorza, A.A., Ferrick, D.A., and Murphy, A.N. (2011). High throughput microplate respiratory measurements using minimal quantities of isolated mitochondria. PLoS One *6*, e21746.

Salabei, J.K., Gibb, A.A., and Hill, B.G. (2014). Comprehensive measurement of respiratory activity in permeabilized cells using extracellular flux analysis. Nat. Protoc. *9*, 421–438.

Simpkins, J.W., Yang, S.H., Sarkar, S.N., and Pearce, V. (2008). Estrogen actions on mitochondria—physiological and pathological implications. Mol. Cell. Endocrinol. *290*, 51–59.

Sims, N.R., and Anderson, M.F. (2008). Isolation of mitochondria from rat brain using Percoll density gradient centrifugation. Nat. Protoc. *3*, 1228–1239.

Sherman, S.P., and Bang, A.G. (2018). High-throughput screen for compounds that modulate neurite growth of human induced pluripotent stem cell-derived neurons. Dis. Model. Mech. https://doi.org/10.1242/dmm.031906.

Tsvetkov, A.S., Miller, J., Arrasate, M., Wong, J.S., Pleiss, M.A., and Finkbeiner, S. (2010). A small-molecule scaffold induces autophagy in primary neurons and protects against toxicity in a Huntington disease model. Proc. Natl. Acad. Sci. U S A *107*, 16982–16987.

Vafai, S.B., and Mootha, V.K. (2012). Mitochondrial disorders as windows into an ancient organelle. Nature *491*, 374–383.

Voccoli, V., and Colombaioni, L. (2009). Mitochondrial remodeling in differentiating neuroblasts. Brain Res. *1252*, 15–29.

Varkuti, B.H., Kepiro, M., Liu, Z., Vick, K., Avchalumov, Y., Pacifico, R., McMullen, C.M., Kamenecka, T.M., Puthanveettil, S.V., and Davis, R.L. (2020). Neuron-based high-content assay and screen for CNS active mitotherapeutics. Sci. Adv. *6*, eaaw8702.

Wagner, B.K., Kitami, T., Gilbert, T.J., Peck, D., Ramanathan, A., Schreiber, S.L., Golub, T.R., and Mootha, V.K. (2008). Large-scale chemical dissection of mitochondrial function. Nat. Biotechnol. *26*, 343–351.

Wang, X., Su, B., Lee, H., Li, X., Perry, G., Smith, M.A., and Zhu, X. (2009). Impaired balance of mitochondria fission and fusion in Alzheimer disease. J. Neurosci. *29*, 9090–9103.

Zorov, D.B., Juhaszova, M., and Sollott, S.J. (2014). Mitochondrial reactive oxygen species (ROS) and ROS-induced ROS release. Physiol. Rev. *94*, 909–950.

Zorova, L.D., Popkov, V.A., Plotnikov, E.Y., Silachev, D.N., Pevzner, I.B., Jankauskas, S.S., Babenko, V.A., Zorov, S.D., Balakireva, A.V., Juhaszova, M., et al. (2018). Mitochondrial membrane potential. Anal. Biochem. *552*, 50–59.

iScience, Volume *23*

Supplemental Information

High-Throughput Small Molecule Screen Identifies Modulators of Mitochondrial Function in Neurons

Boglarka H. Varkuti, Ze Liu, Miklos Kepiro, Rodrigo Pacifico, Yunchao Gai, Ted Kameneka, and Ronald L. Davis

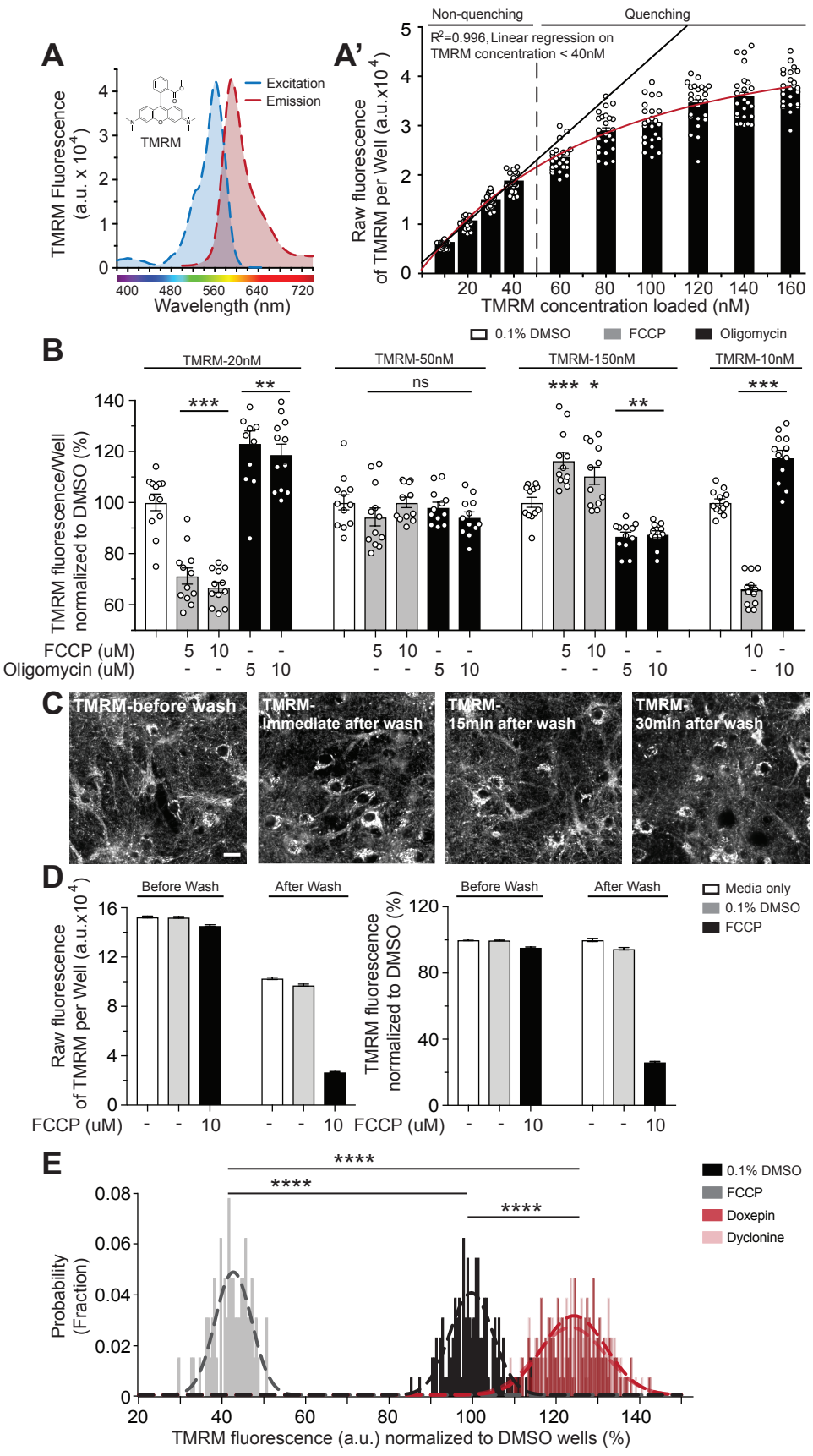
A
TMRM Fluorescence (a.u. x 10^4)
Excitation
Emission
TMRM
Wavelength (nm)
A'
Non-quenching
Quenching
R²=0.996, Linear regression on TMRM concentration < 40nM
Raw fluorescence of TMRM per Well (a.u.x10^4)
TMRM concentration loaded (nM)
B
0.1% DMSO
FCCP
Oligomycin
TMRM-20nM
TMRM-50nM
TMRM-150nM
TMRM-10nM
TMRM fluorescence/Well normalized to DMSO (%)
FCCP (uM)
Oligomycin (uM)
C
TMRM-before wash
TMRM-immediate after wash
TMRM-15min after wash
TMRM-30min after wash
D
Before Wash
After Wash
Raw fluorescence of TMRM per Well (a.u.x10^4)
TMRM fluorescence normalized to DMSO (%)
FCCP (uM)
Media only
0.1% DMSO
FCCP
E
0.1% DMSO
FCCP
Doxepin
Dyclonine
Probability (Fraction)
TMRM fluorescence (a.u.) normalized to DMSO wells (%)

Figure S1. Development of the high-throughput TMRM assay. Related to Figure 1.
(A) TMRM fluorescence. The excitation and emission spectra of TMRM. **(A')** TMRM fluorescence as a function of concentration in primary neuronal cultures. DIV14 neurons were loaded with TMRM with serial concentrations from 10 to 160 nM. After 6h of incubation, neurons were washed briefly, and the intra-mitochondrial fluorescence was measured. TMRM fluorescence increased linearly with increased concentration below 40 nM in the medium. High concentrations within mitochondria triggered self-quenching effects and a deviation from linearity. The mitochondrial TMRM fluorescence across TMRM concentration was fit to a hyperbolic function. Bar plots represent the mean ± the SEM.
(B) Quenching and non-quenching concentrations of TMRM in primary neuronal cultures. DIV14 neurons were loaded with TMRM at 10, 20, 50 and 150 nM for 3h and then treated for 5-10m with DMSO (0.1%), the ionophore FCCP (5 and 10 μM) or the ATP synthase inhibitor oligomycin (5 and 10 μM). Cells were washed and the intracellular TMRM intensity was measured. $\Delta\Psi_m$ hyperpolarization by oligomycin triggered further accumulation of mitochondrial TMRM, thus a further self-quenching effect and decreased fluorescence at high concentrations (150 nM), but increased fluorescence at non-quenching concentrations (10 and 20 nM). In contrast, FCCP collapses $\Delta\Psi_m$ and releases mitochondrial TMRM, producing a transient increase of fluorescence at quenching concentrations (150 nM) and a decrease in fluorescence at non-quenching concentrations (10 and 20 nM). Bar plots represent the mean of well fluorescence intensity ± the SEM normalized to DMSO-treated wells (n=12). One-way ANOVA followed by Dunn's *post hoc* for each concentration of TMRM. * P<0.05, ** P<0.01 and *** P<0.001 compared to each DMSO control**.**
(C) TMRM assay wash steps do not affect the integrity of the cultured neurons. Representative images of TMRM labeled primary neurons before and 0, 15, and 30m after washing steps, showing that the wash steps neither disturb the cell layer nor alter the morphology of neurons and mitochondria. Scale bar = 20 μm.
(D) TMRM wash steps are required for an accurate determination of mitochondrial associated TMRM fluorescence. The raw (left) and normalized (right; normalized to each of the DMSO controls) TMRM signal in untreated, DMSO- and FCCP-treated wells, pre- and post-washing steps. Wash steps remove about 40% of the total fluorescence due to the removal of free TMRM in the medium, indicating that approximately 60% of the TMRM is sequestered in mitochondria. FCCP collapses $\Delta\Psi_m$, strongly reducing the mitochondrial signal in the washed wells but not in those measured before wash. Bar plots represent the mean ± the SEM.
(E) Distribution of TMRM fluorescence in neurons treated with positive hits (red), DMSO (black) and the negative control, FCCP (gray). DIV13 neurons were incubated with DMSO (0.1%), FCCP (12.5 μM) and the selected hits, dyclonine (12.5 μM) or doxepin (12.5 μM), for 24h and the $\Delta\Psi_m$ measured by whole well TMRM fluorescence. The results are presented as %TMRM fluorescence relative to the in-plate DMSO control which was normalized to 100%. n=128 wells for each group; *P<0.05, **P<0.01, ***P<0.001, ****P<0.0001 compared with DMSO-treated controls, one-way ANOVA followed by Dunn's *post-hoc*.

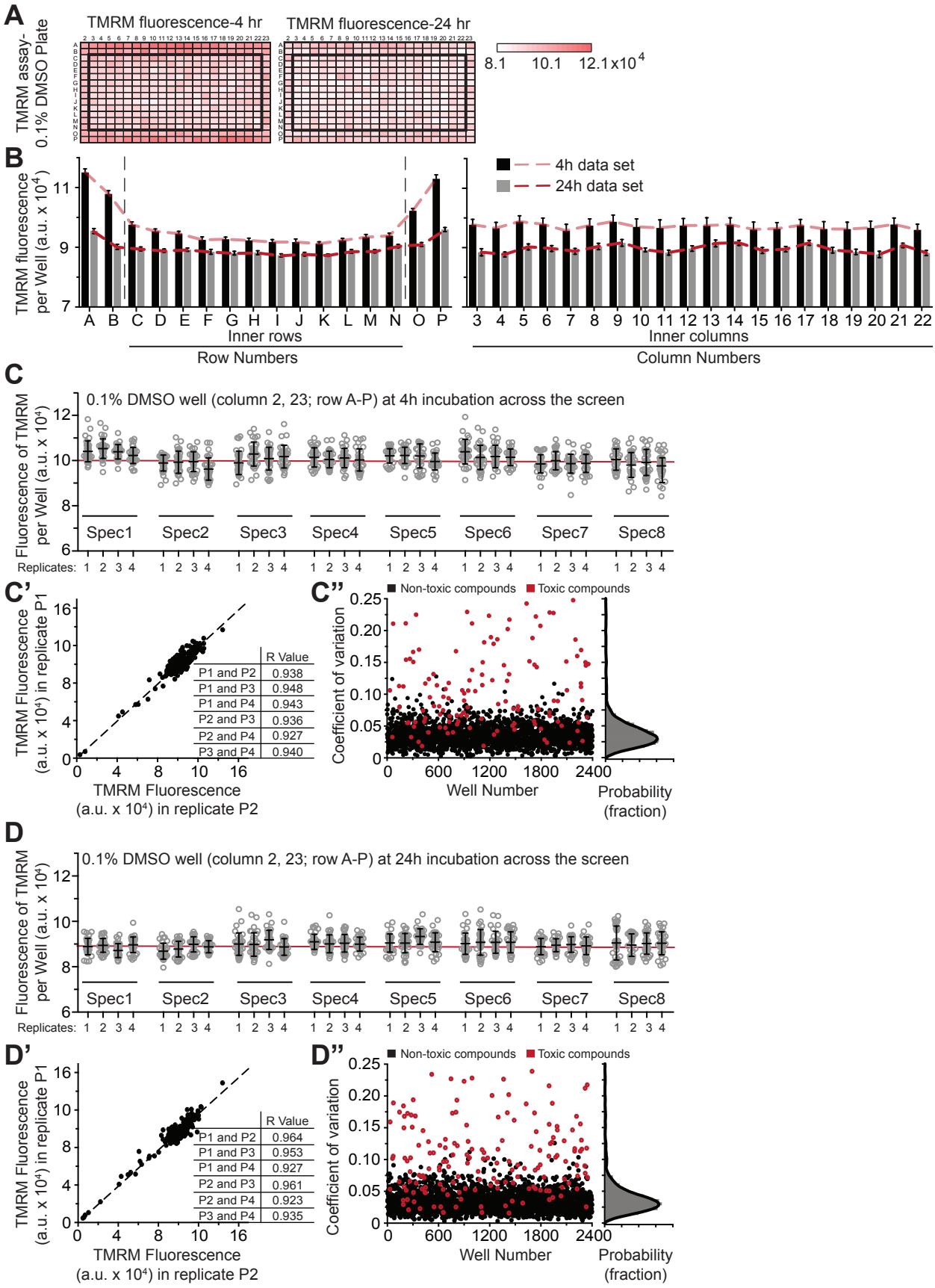
A
TMRM assay-
0.1% DMSO Plate
TMRM fluorescence-4 hr
TMRM fluorescence-24 hr
8.1
10.1
12.1x10^4
B
TMRM fluorescence
per Well (a.u. x 10^4)
4h data set
24h data set
Inner rows
Row Numbers
Inner columns
Column Numbers
C
0.1% DMSO well (column 2, 23; row A-P) at 4h incubation across the screen
Fluorescence of TMRM
per Well (a.u. x 10^4)
Spec1
Spec2
Spec3
Spec4
Spec5
Spec6
Spec7
Spec8
Replicates:
C'
TMRM Fluorescence
(a.u. x 10^4) in replicate P1
TMRM Fluorescence
(a.u. x 10^4) in replicate P2
R Value
P1 and P2 0.938
P1 and P3 0.948
P1 and P4 0.943
P2 and P3 0.936
P2 and P4 0.927
P3 and P4 0.940
C''
Non-toxic compounds
Toxic compounds
Coefficient of variation
Well Number
Probability
(fraction)
D
0.1% DMSO well (column 2, 23; row A-P) at 24h incubation across the screen
D'
R Value
P1 and P2 0.964
P1 and P3 0.953
P1 and P4 0.927
P2 and P3 0.961
P2 and P4 0.923
P3 and P4 0.935
D''

Figure S2. Plate edge effects. Related to Figure 1.

(A) Plate edge effects. In a pilot experiment using two plates with wells treated only with the carrier DMSO, we observed significant edge effects on TMRM fluorescence, with elevated signal in the outer two rows or columns but relatively homogenous signals across the population of inner wells. Heat maps of TMRM fluorescence from columns 2-23 of DMSO treated plates at 4 and 24h of incubation. The fluorescence is the average per well across two independent plates. Primary neurons in 384-well plates were cultured to DIV13 and incubated with TMRM (10 nM) and DMSO (final concentration 0.1%) in all wells. The TMRM intensity was assayed in a plate reader at 4 and 24h after the necessary washing steps. No TMRM dye was added in columns 1 and 24 (not illustrated). The auto-fluorescence of the neurons and plastics in the plate bottom in these wells was measured as background and subtracted from the wells to which TMRM was added. The black box represents the "inner wells" used for the screen.

(B) TMRM plate row and column effects. The average whole well TMRM fluorescence across rows and columns at 4 and 24h. Significant edge-effects were observed across rows A-P, with the outer two rows exhibiting significantly increased TMRM fluorescence relative to inner rows. Data plotted as mean ± std. To compensate for the significant edge effects, data generated from the outer rows (rows A,B,O,P) and inner wells (rows C-N, columns 3-22) were analyzed separately for the primary screen as described below. The outer rows A, B, O and P were not used for the subsequent rescreen and dose response experiments. Bar plots represent the mean ± the SEM.

(C, D) TMRM assay variability across plates. The MicroSource Spectrum library compounds were pintooled from source plate rows A-P, columns 3-22, and DMSO from a source plate rows A-P, columns 2 and 23. The basal TMRM fluorescence was measured from 32 DMSO (0.1%) control wells in columns 2 and 23 on each plate to monitor variability across the screen. There was no significant difference in average TMRM fluorescence of the DMSO-treated wells at 4 **(C)** or 24h **(D)** of incubation across the four replicates for each of the eight source plates (Spec 1-8). In addition, no significant signal drift was observed from the first to the last plate throughout the primary screen indicating consistency in the primary neuron cultures and assay. Points represent individual wells and the bars represent the mean ± std. The red horizontal line indicates the basal TMRM fluorescence at 4 **(C)** or 24h **(D)** of incubation, measured from DMSO-treated wells and calculated as the mean across all plates used in the primary screen. This mean showed a ~10% reduction between 4 and 24h of incubation. **(C'-D')** Representative correlation plots of TMRM signals for compound-treated wells of replicates plates 1 (P1) and 2 (P2) for Spectrum source plate 4. The table inset shows the high correlation (R values > 0.92) for all *inter se* comparisons among replicate plates. **(C", D")** The Coefficient of Variation (CV) of four replicates for each of the 2400 compound-treated wells was individually plotted to illustrate variation across replicates. The CV was centered around 3% and was generally <8% for almost all nontoxic compounds. Higher CV values were observed in wells treated with toxic compounds (red).

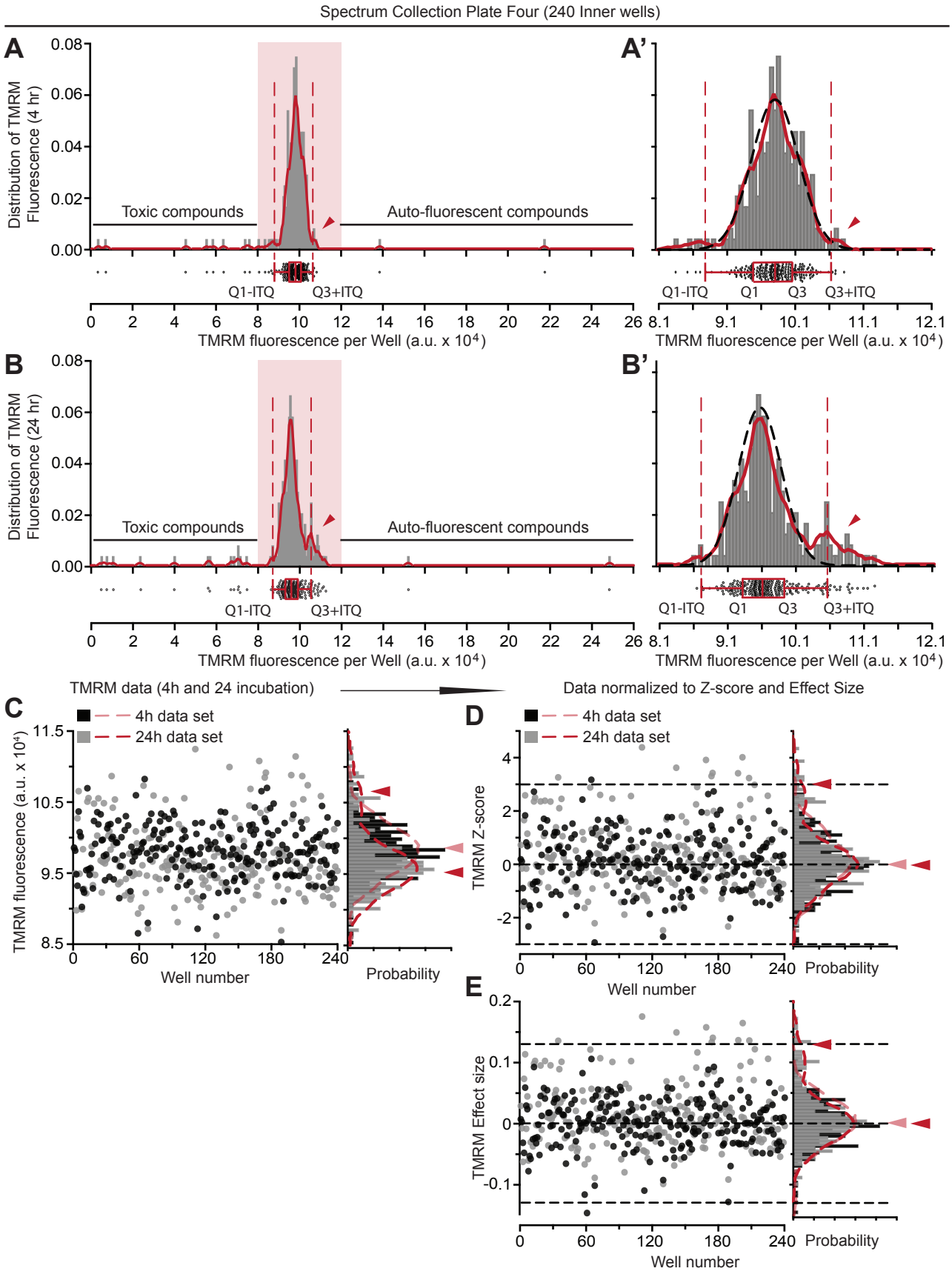
Spectrum Collection Plate Four (240 Inner wells)
A
A'
B
B'
Distribution of TMRM Fluorescence (4 hr)
Distribution of TMRM Fluorescence (24 hr)
Toxic compounds
Auto-fluorescent compounds
Q1-ITQ
Q3+ITQ
Q1
Q3
TMRM fluorescence per Well (a.u. x 10⁴)
TMRM data (4h and 24 incubation)
Data normalized to Z-score and Effect Size
C
D
E
4h data set
24h data set
TMRM fluorescence (a.u. x 10⁴)
TMRM Z-score
TMRM Effect size
Well number
Probability

Figure S3. Population control for data normalization of TMRM fluorescence. Related to Figure 1.
(A, B) Population control for data normalization of TMRM fluorescence. We used a "non-DMSO-control" statistical approach to normalize raw TMRM fluorescence into Z scores and Effect-Size (fold change) for hit identification, based on the fact that the majority of small molecules in HTS assays are absent of biological effects, thus serving as "within plate controls" (Brideau et al., 2003; Malo et al., 2006). Distribution of TMRM fluorescence from 240 inner wells treated with compounds from source plate 4 at 4 **(A)** and 24h **(B)** showing that most of the wells fall into a normal distribution and can be considered to consist of inactive compounds. Some compounds in the inner wells dramatically reduced the TMRM signal and were classified as toxic compounds; others were identified as auto-fluorescent. The wells containing these compounds were not included in the "inactive" population. The plots in **(A', B')** expand the red-highlighted region in **(A, B).** A bimodal distribution (red line), most obvious in the 24h data set was observed, identifying putative hits in the shoulder peak. The TMRM fluorescence of "inactive" compounds within the dominant peak showed a similar plate mean (μ_{plate}) and standard derivation (σ_{plate}) calculated from inner DMSO-wells in parallel DMSO-only treated plates. This "inactive" population from each plate was used for data normalization. Statistically, this subpopulation was defined by using Tukey's fences rule based on the interquartile range **(A', B')**. The black dotted line shows the normal distribution of the "inactive" subpopulation with TMRM readouts in the range of [Q1-(Q3-Q1/ITQ), Q3+(Q3-Q1)]. Compounds with activity outside of this range were identified as outliers; Q1 and Q3 represent the first (lower) and third (upper) quartiles respectively. A modified box-and-whiskers plot is illustrated below each distribution. Boxes represent the interquartile range, lines within boxes are medians, whiskers represent values of 1.0 x (interquartile range/ITQ: Q3-Q1) from the first (Q1) and third (Q3) quartiles.
(C-E) TMRM assay Z-scores and effect size. The plate mean (μ_{plate}) and standard deviation (σ_{plate}) were calculated using the subpopulation trimmed of outliers to normalize compound performance as Z-scores and Effect Size. Z-scores were calculated by subtracting the μ_{plate}, then dividing by the σ_{plate} (($value_{compound}$-μ_{plate})/σ_{plate}). Effect size was calculated by subtracting the μ_{plate}, then dividing by the μ_{plate} to obtain fold change (($value_{compound}$ - μ_{plate})/μ_{plate}). Putative hits from the primary screen were identified as enhancing the well fluorescence above the μ_{plate} by $3\sigma_{plate}$ for inner wells, and by $2.5\sigma_{plate}$ for outer wells (Figure 1C-D).

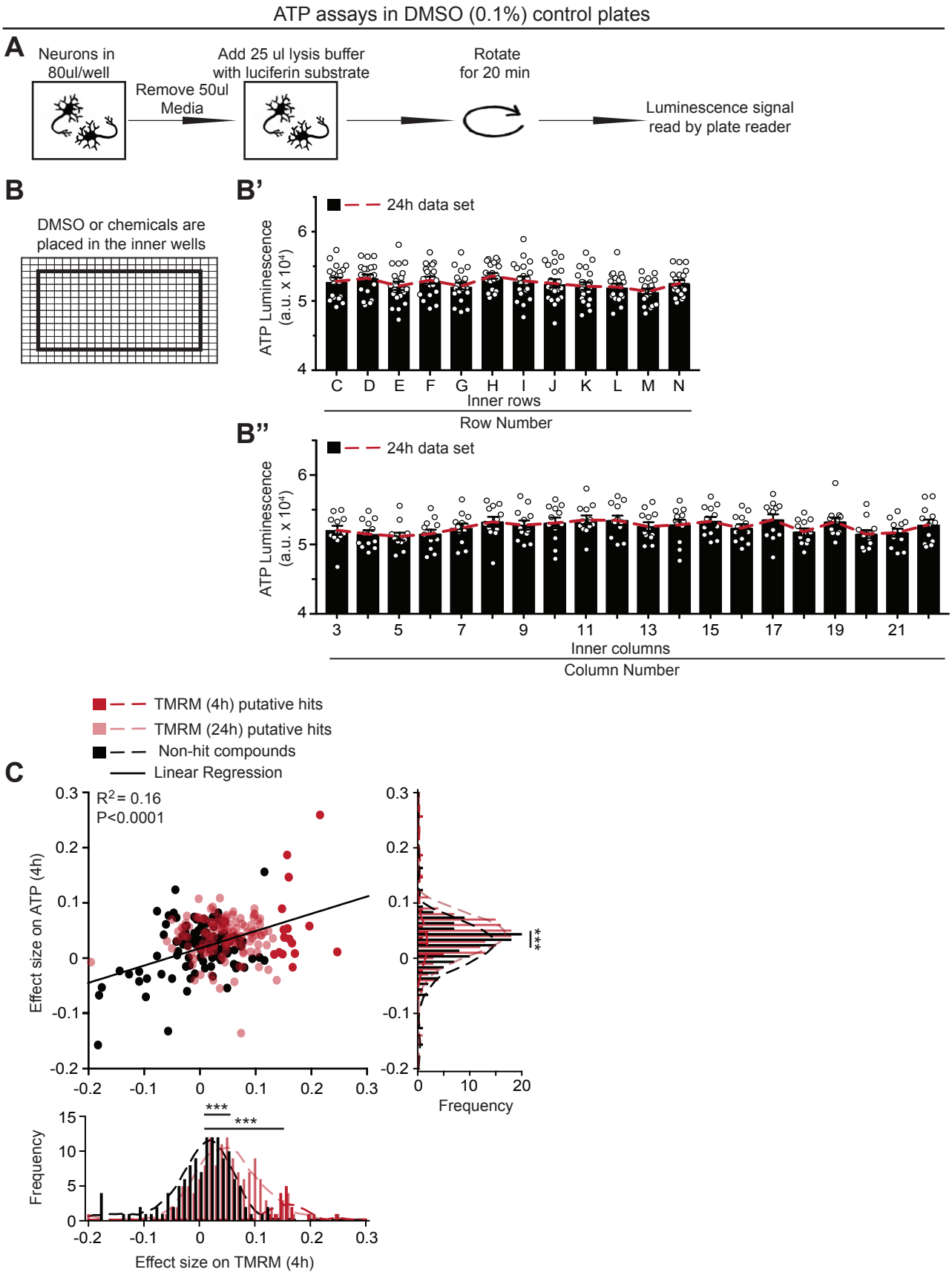
ATP assays in DMSO (0.1%) control plates
A
Neurons in 80ul/well
Remove 50ul Media
Add 25 ul lysis buffer with luciferin substrate
Rotate for 20 min
Luminescence signal read by plate reader
B
DMSO or chemicals are placed in the inner wells
B'
24h data set
ATP Luminescence (a.u. x 10⁴)
C D E F G H I J K L M N
Inner rows
Row Number
B''
24h data set
ATP Luminescence (a.u. x 10⁴)
3 5 7 9 11 13 15 17 19 21
Inner columns
Column Number
C
TMRM (4h) putative hits
TMRM (24h) putative hits
Non-hit compounds
Linear Regression
R² = 0.16
P<0.0001
Effect size on ATP (4h)
Frequency
***
Effect size on TMRM (4h)

Figure S4. ATP assay. Related to Figure 1.

(A) Schematic illustration of the luminescence-based ATP assay in the 384-well plate format.

(**B-B**") Testing the assay using a DMSO source plate. 100 nl DMSO (final concentration ~0.1%) was pintooled into the inner wells of a 384 well microplate. Cellular ATP was measured using the CellTiter-Glo® luminescence assay (Promega) and the well luminescence measured. The signal of DMSO-treated wells was aggregated by column (**B'**) or by row (**B"**) and plotted. No significant difference in the average luminescence of DMSO wells across the inner columns or rows (one-way ANOVA) was found. Bar plots represent the mean ± the SEM.

(C) Orthogonal screen of putative TMRM hits measuring ATP production. 16 putative hits with effects at 4h (red), and 135 putative hits with effects at 24h (pink) from the primary screen were tested for ATP production alongside 134 randomly selected non-hit compounds (black) and 40 DMSO controls. The main plot shows the correlation of the effect size of TMRM fluorescence and ATP production in wells after 4h of incubation for these compounds. The black line represents the fit using a linear regression model using all plotted compounds (R^2 =0.16, p<0.0001). The compound-induced effect size on ATP production (right histogram) at 4h was normalized to the mean value of the 40 "within-plate" DMSO controls as ($value_{compound}$ - μ_{DMSO})/μ_{DMSO}. The population of 24h TMRM hits was significantly different from the non-hit population for ATP effect size (right histogram). The 24 and 4h TMRM hit populations were significantly different from the non-hit population for TMRM fluorescence effect size (bottom histogram). The 4h TMRM hits showed a large variation in their effect size on ATP levels (note the distribution of 4h TMRM points), suggesting that acute increases in $\Delta\Psi_m$ only weakly correlate with effects on ATP generation. One-way ANOVA followed by Dunn's *post hoc* to compare among groups, confidence levels were set at **P*<0.05, ***P*<0.01, ****P*<0.001.

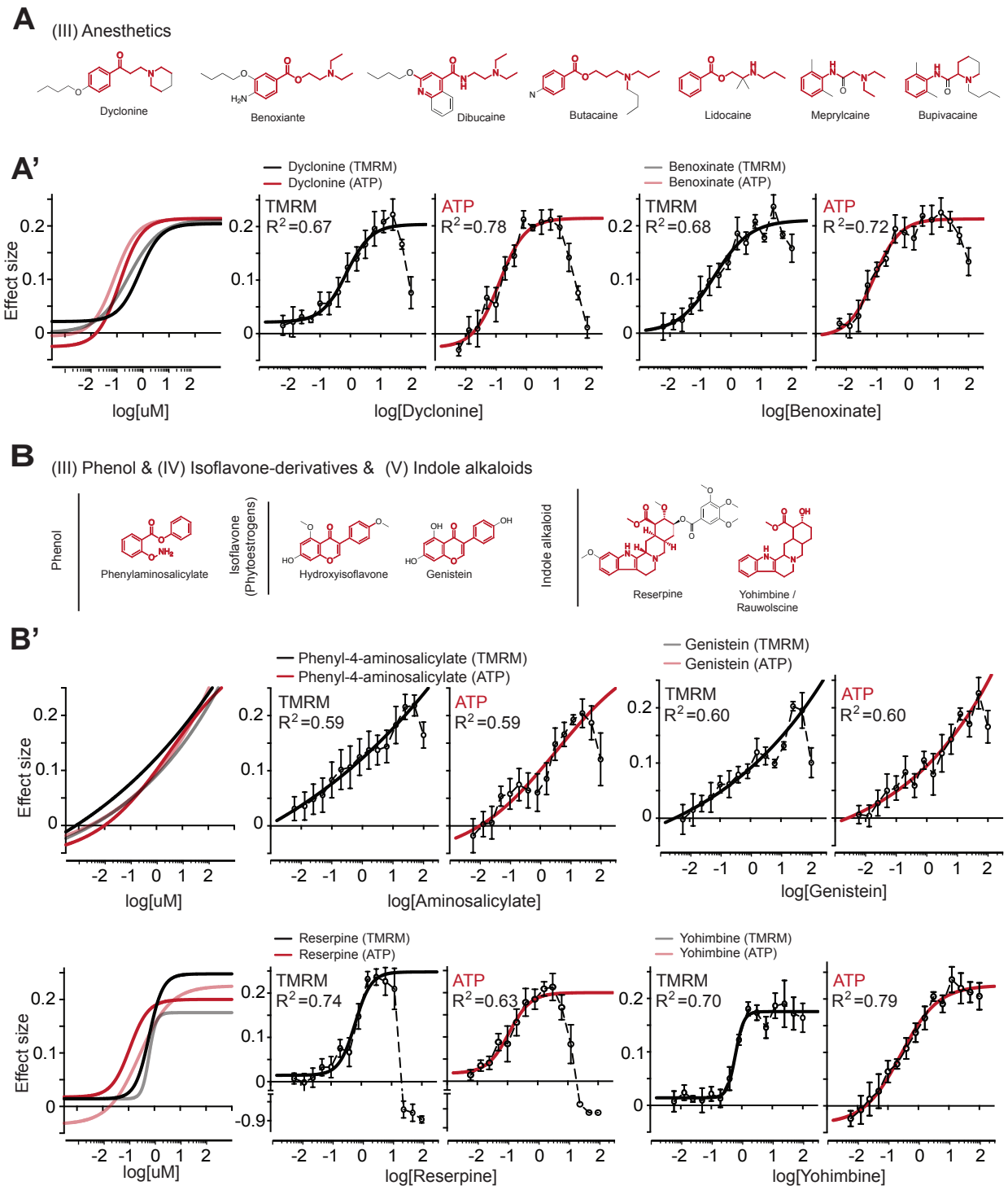

Figure S5. Dose response results for functional modulators of neuronal mitochondria. Related to Figure 2.

Dose response assays of compounds in clusters with structural similarity. The 2D-structures of the compounds are displayed **(A,B)** with the common core scaffold highlighted in red. We used 15 concentrations from 6 nM to 100 uM for the assays. Points represent the mean ± SEM of 6 independent experiments, with each compound tested in duplicate in each experiment. EC_{50} values were calculated from the fitted logistic curve (see Table S2). A summary of the dose response curves for compounds tested for both TMRM fluorescence and ATP generation is illustrated at the left for each group for visualizing and comparing the magnitude of TMRM and ATP effect size.

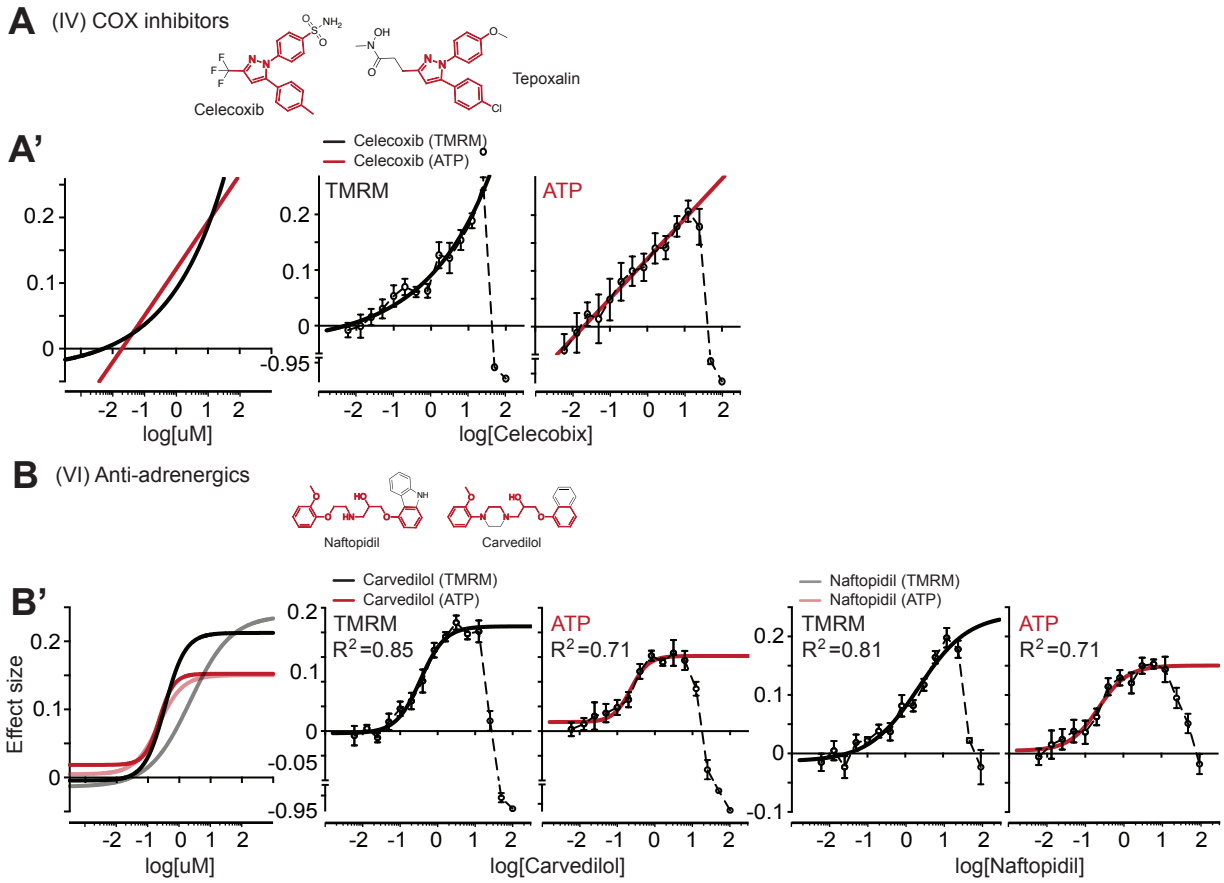

Figure S6. Dose response results for functional modulators of neuronal mitochondria. Related to Figure 2.

Dose response assays of compounds in clusters with structural similarity. The 2D-structures of the compounds are displayed **(A,B)** with the common core scaffold highlighted in red. We used 15 concentrations from 6 nM to 100 uM for the assays. Points represent the mean ± SEM of 6 independent experiments, with each compound tested in duplicate in each experiment. EC_{50} values were calculated from the fitted logistic curve (see Table S2). A summary of the dose response curves for compounds tested for both TMRM fluorescence and ATP generation is illustrated at the left for each group for visualizing and comparing the magnitude of TMRM and ATP effect size.

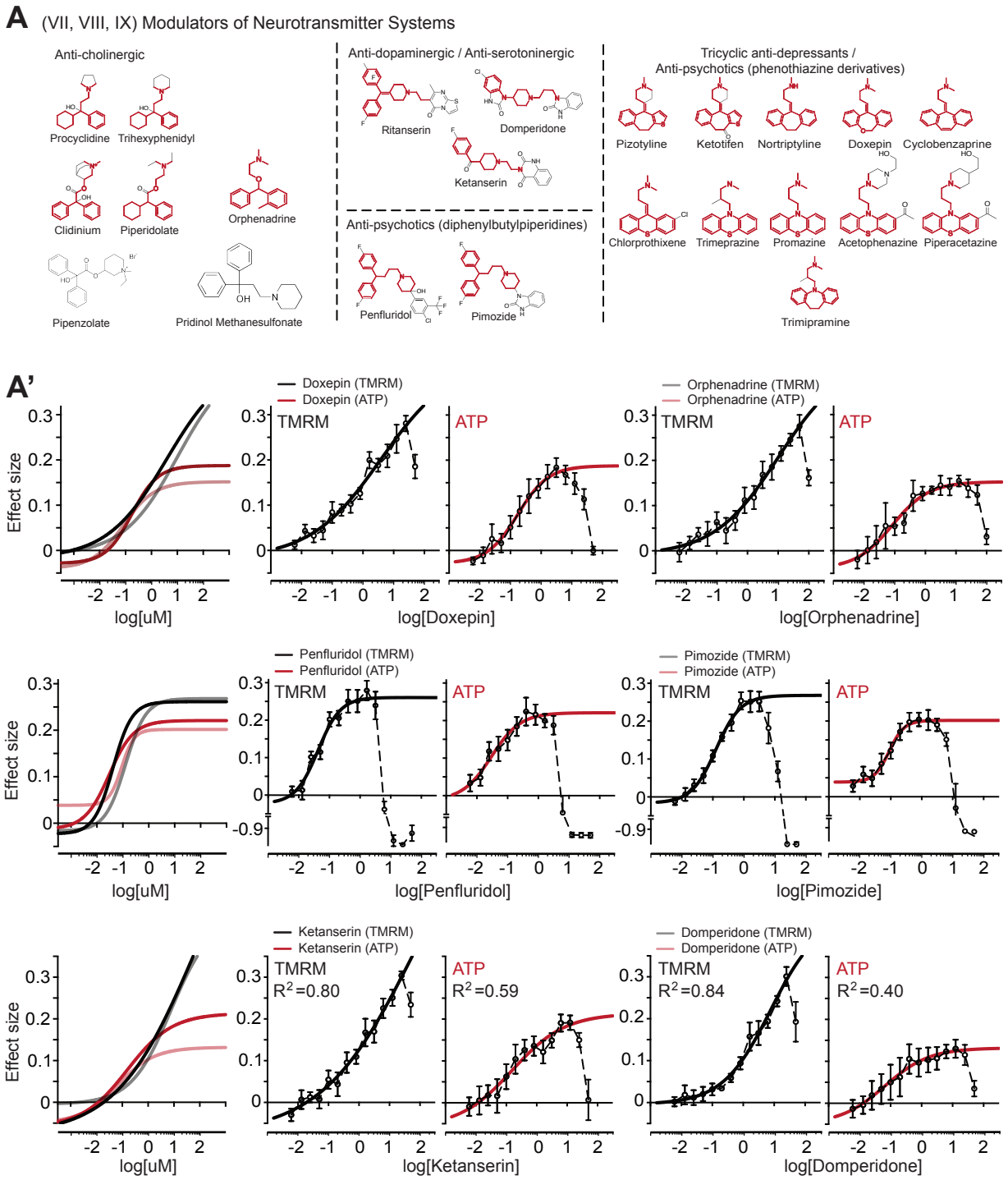

Figure S7. Dose response results for functional modulators of neuronal mitochondria. Related to Figure 2.

Dose response assays of compounds in clusters with structural similarity. The 2D-structures of the compounds are displayed **(A)** with the common core scaffold highlighted in red. We used 15 concentrations from 6 nM to 100 uM for the assays. Points represent the mean ± SEM of 6 independent experiments, with each compound tested in duplicate in each experiment. EC_{50} values were calculated from the fitted logistic curve (see Table S2). A summary of the dose response curves for compounds tested for both TMRM fluorescence and ATP generation is illustrated at the left for each group for visualizing and comparing the magnitude of TMRM and ATP effect size.

Compound Name	TMRM Primary	TMRM Rescreen	ATP
1. *AZELASTINE HYDROCHLORIDE*	7.06	6.13	5.30
2. *PIZOTYLINE MALATE*	3.21	5.84	7.13
3. *DOXEPIN HYDROCHLORIDE*	3.44	5.41	7.03
4. *TRIMIPRAMINE MALEATE*	5.18	5.16	5.24
5. *ORPHENADRINE CITRATE*	3.26	5.75	6.08
6. *NORTRIPTYLINE HYDROCHLORIDE*	3.77	5.25	5.66
7. *CYCLIZINE*	3.41	5.91	5.18
8. *KETOTIFEN FUMARATE*	3.91	3.98	5.58
9. *CHLORPROTHIXENE HYDROCHLORIDE*	6.17	5.04	3.17
10. *PIMETHIXENE MALEATE*	3.95	5.12	4.56
11. *DIMENHYDRINATE*	3.98	4.31	4.94
12. *CYCLOBENZAPRINE HYDROCHLORIDE*	5.52	4.71	3.49
13. *CLEMIZOLE HYDROCHLORIDE*	3.54	5.90	4.16
14. *TRIMEPRAZINE TARTRATE*	3.13	3.94	5.75
15. *PROMAZINE HYDROCHLORIDE*	3.81	4.04	4.76
16. *CLOZAPINE*	3.24	5.80	3.88
17. *THONZYLAMINE HYDROCHLORIDE*	3.16	3.21	5.17
18. *CHLOROPYRAMINE HYDROCHLORIDE*	3.35	5.24	3.26
19. *TRIHEXYPHENIDYL HYDROCHLORIDE*	6.07	7.08	5.95
20. *PROCYCLIDINE HYDROCHLORIDE*	4.55	6.91	7.14
21. *PRIDINOL METHANESULFONATE*	5.88	6.92	5.46
22. *DROFENINE HYDROCHLORIDE*	3.68	5.96	4.84
23. *CLIDINIUM BROMIDE*	2.49	4.11	6.21
24. *PIPERIDOLATE HYDROCHLORIDE*	3.58	3.76	5.72
25. *PIPENZOLATE BROMIDE*	3.14	7.09	3.45
26. *ADIPHENINE HYDROCHLORIDE*	3.05	3.21	4.95
27. *DYCLONINE HYDROCHLORIDE*	3.64	6.30	7.04
28. *DIBUCAINE HYDROCHLORIDE*	3.83	6.82	6.22
29. *BENOXINATE HYDROCHLORIDE*	3.62	6.64	5.57
30. *HYCANTHONE*	4.40	5.48	4.61
31. *TOLPERISONE HYDROCHLORIDE*	3.57	3.67	5.49
32. *PROPARACAINE HYDROCHLORIDE*	3.43	4.65	4.11
33. *5alpha-CHOLESTAN-3beta-OL-6-ONE*	7.10	7.61	5.86
34. *CYCLOPAMINE*	3.74	8.14	5.15
35. *ANDROSTERONE*	3.77	4.76	5.63
36. *5,4'-DIMETHOXY-7-HYDROXYISOFLAVONE*	5.24	6.90	5.76
37. *PHENYL AMINOSALICYLATE*	4.63	4.94	7.48
38. *GENISTEIN*	3.38	4.21	5.96
39. *APIGENIN DIMETHYL ETHER*	3.69	5.03	4.73
40. *KETANSERIN TARTRATE*	5.62	5.26	5.68
41. *RITANSERIN*	5.25	5.83	4.40
42. *DOMPERIDONE*	3.33	5.58	5.20
43. *PIMOZIDE*	2.65	3.74	6.60
44. *CARVEDILOL PHOSPHATE*	5.81	5.43	6.87
45. *NAFTOPIDIL*	3.64	9.07	3.62
46. *CARVEDILOL*	4.11	5.71	5.32
47. *ACETOPHENAZINE MALEATE*	5.64	5.34	5.65
48. *PIPERACETAZINE*	5.30	5.01	5.80

49. *THIOTHIXENE*	3.08	3.38	3.80
50. *DIHYDROFISSINOLIDE*	3.94	4.61	5.15
51. *1,7-DIDEACETOXY-1,7-DIOXO-3-DEACETYLKHIVORIN*	3.65	4.00	5.46
52. *CARAPIN-8(9)-ENE*	3.50	3.82	4.89
53. *YOHIMBINE HYDROCHLORIDE*	2.70	5.70	3.11
54. *RAUWOLSCINE HYDROCHLORIDE*	4.30	8.77	8.40
55. *RESERPINE*	7.44	7.89	5.29
56. *DEXPROPRANOLOL HYDROCHLORIDE [R(+)]*	4.37	4.79	6.22
57. *PROPRANOLOL HYDROCHLORIDE (+/-)*	4.03	3.07	5.06
58. *LIDOCAINE HYDROCHLORIDE*	3.06	4.69	6.98
59. *BUPIVACAINE HYDROCHLORIDE*	5.35	5.25	4.80
60. *TOREMIFENE CITRATE*	3.31	7.05	3.29
61. *CLOMIPHENE CITRATE*	2.94	3.45	4.20
62. *ESTRADIOL METHYL ETHER*	3.74	3.55	4.80
63. *ESTRONE ACETATE*	3.26	5.89	3.36
64. *CELECOXIB*	6.67	4.72	7.57
65. *DIPERODON HYDROCHLORIDE*	3.75	6.07	8.02
66. *VINPOCETINE*	5.76	6.16	6.29
67. *NEFAZODONE HYDROCHLORIDE*	4.00	6.11	6.30
68. *BUTACAINE SULFATE*	3.85	5.06	6.99
69. *NEBIVOLOL HYDROCHLORIDE*	3.73	5.29	6.92
70. *LOBELINE HYDROCHLORIDE*	6.62	6.75	3.67
71. *INDOLE-3-CARBINOL*	3.15	6.27	6.52
72. *TRIMEBUTINE MALEATE*	3.79	5.82	6.14
73. *TEPOXALIN*	4.36	3.75	6.89
74. *MEPRYLCAINE HYDROCHLORIDE*	3.56	5.91	6.05
75. *NIMODIPINE*	4.40	3.98	6.53
76. *PENFLURIDOL*	4.29	4.83	5.75
77. *BISPHENOL A*	3.35	7.40	4.73
78. *NAFRONYL OXALATE*	4.08	5.89	5.17
79. *DOXAZOSIN MESYLATE*	4.39	5.94	4.68
80. *BENZONATATE*	2.78	8.21	4.35
81. *TIGECYCLINE*	3.91	5.95	4.97
82. *AJMALINE*	3.76	6.40	4.76
83. *PYRIMETHAMINE*	3.43	4.00	6.54
84. *EXALAMIDE*	3.39	4.57	6.10
85. *HYDROXYZINE PAMOATE*	3.15	6.04	5.22
86. *MEFLOQUINE*	3.75	5.54	5.09
87. *TILETAMINE HYDROCHLORIDE*	3.31	4.20	6.27
88. *AMBROXOL HYDROCHLORIDE*	4.00	5.14	5.04
89. *COLISTIN SULFATE*	3.27	5.24	5.48
90. *HETEROPEUCENIN, METHYL ETHER*	3.45	4.33	5.92
91. *PROPAFENONE HYDROCHLORIDE*	3.75	5.04	5.18
92. *QUININE ETHYL CARBONATE*	4.64	6.26	3.60
93. *ARIPIPRAZOLE*	2.98	7.76	3.66
94. *FULVESTRANT*	3.31	6.27	4.27
95. *BUSSEIN*	3.44	3.92	5.58
96. *CANAGLIFLOZIN*	4.55	6.36	3.13

97. *ALVERINE CITRATE*	4.24	4.15	4.56
98. *DOXORUBICIN*	4.02	5.05	4.00
99. *SCLAREOL*	2.80	5.41	4.64
100. *IMIDAZOL-4-YLACETIC ACID SODIUM SALT*	3.58	4.56	4.61
101. *OXICONAZOLE NITRATE*	3.08	3.28	5.76
102. *NAFTIFINE HYDROCHLORIDE*	3.26	4.64	4.65
103. *SERTRALINE HYDROCHLORIDE*	3.42	4.15	4.82
104. *1-HYDROXY-3,6,7-TRIMETHOXY-2,8-DIPRENYLXANTHONE*	3.34	3.27	5.44
105. *DEHYDROABIETAMIDE*	3.42	5.12	4.15
106. *EUGENOL*	4.17	3.10	4.39
107. *PENBUTOLOL SULFATE*	3.16	5.35	3.39
108. *PAROXETINE HYDROCHLORIDE*	3.53	3.26	4.41
109. *BUTYL PARABEN*	3.42	4.18	3.84
110. *TRICLABENDAZOLE*	3.30	3.61	3.97
111. *CLEMASTINE FUMARATE*	2.82	3.22	4.56
112. *LEVOMILNACIPRAN HYDROCHLORIDE*	3.26	3.53	3.87
113. *SODIUM NITROPRUSSIDE*	3.38	3.22	2.90
114. *MEDROXYPROGESTERONE ACETATE*	3.66	3.67	2.64
115. *ESTRADIOL CYPIONATE*	2.59	4.67	2.98
116. *AVANAFIL*	3.13	3.42	1.30
117. *TERCONAZOLE*	5.15	5.95	2.82
118. *OXELAIDIN CITRATE*	4.27	6.44	2.73
119. *ESTRIOL BENZYL ETHER*	3.17	6.67	2.03
120. *LARIXOL ACETATE*	3.96	5.67	2.67
121. *AMITRIPTYLINE HYDROCHLORIDE*	4.78	1.81	4.82
122. *IMIPRAMINE HYDROCHLORIDE*	3.31	0.91	5.10
123. *BENAZEPRIL HYDROCHLORIDE*	3.43	2.43	5.26
124. *FLUOXETINE HYDROCHLORIDE*	3.42	1.87	3.70
125. *ORLISTAT*	3.43	1.56	2.36
126. *BIFONAZOLE*	3.81	1.84	4.00
127. *FELODIPINE*	3.80	2.41	5.08
128. *ANCITABINE HYDROCHLORIDE*	3.04	1.36	0.14
129. *PHYTOL*	3.42	2.70	4.63
130. *4'-METHOXYCHALCONE*	3.42	1.48	3.97
131. *DESOXYCORTICOSTERONE ACETATE*	2.81	1.08	3.62
132. *SPARTEINE SULFATE*	2.65	1.95	2.92
133. *CHLORPROMAZINE*	2.79	2.66	5.00
134. *NICARDIPINE HYDROCHLORIDE*	4.22	-5.52	-3.75
135. *PRAMOXINE HYDROCHLORIDE*	2.93	-4.72	-1.97

Table S1. Z-scores for hits from the TMRM and ATP screen. Related to Figures 1 and 2. Listing of the 135 putative hits with Z-scores from the primary screen when assayed at 24h (TMRM Primary, hits: >3 Z-scores for inner wells, >2.5 Z-scores for outer wells), from the rescreen (TMRM Rescreen, hits: >3 Z-scores) and from the ATP orthogonal screen (ATP, hits with >3 Z-scores). Bolded compounds were hits when assayed at 4h as well in the 24h primary screen. Primary hits that were confirmed in the rescreen (120) are listed above the bold line. The 112 hits from the ATP orthogonal screen are listed above the dashed line.

Cluster	Compound	TMRM-EC_{50} (nM)	ATP-EC_{50} (nM)	TMRM (Effect-size)	ATP (Effect-size)	OCR	Mitochondrial Morphology	Neurite Area	Luperox insult	3xTG genetic background
Oral/Local Anesthetic (cluster 3)	Dyclonine	750	140	22.0%	20.7%	increased	elongated	increased	rescues	rescues
	Benoxinate	490	80	21.0%	21.4%	-	elongated	n.s.	rescues	rescues
	Lidocaine	1890	110	17.4%	15.8%	-	-	-	rescues	rescues
Antibiotic (cluster 3)	Phenyl-4-amino salicylate	1800	2020	21.8%	20.4%	-	elongated	n.s.	rescues	rescues
Isoflavone (cluster 4)	Genistein	1300	3000	19.5%	20.6%	-	elongated	n.s.	rescues	rescues
COX Inhibitor (cluster 4)	Celecoxib	5180	490	27.5%	20.7%	-	elongated	n.s.	no rescue	rescues
Indole Alkaloids (cluster 5)	Yohimbine	620	270	18.6%	23.6%	increased	elongated	increased	rescues	rescues
	Rauwolscine	4580	1000	29.4%	20.9%	-	-	-	-	-
	Reserpine	640	120	22.5%	20.5%	-	-	-	-	-
Adrenergic Antagonists (cluster 6)	Carvedilol	350	230	20.2%	15.9%	-	-	-	-	-
	Naftopidil	2240	230	18.8%	15.0%	-	-	-	-	-
Anti-psychotics Dopamine Serotoninergic Antagonists (cluster 7)	Penfluridol	50	30	25.2%	22.4%	-	elongated	increased	no rescue	rescues
	Pimozide	130	90	25.1%	20.4%	-	elongated	increased	rescues	rescues
	Ketanserin	1300	160	30.0%	19.1%	-	-	-	-	-
	Domperidone	1800	65	28.3%	13.0%	-	-	-	-	-
Tricyclic Antidepressant (clusters 7 and 8)	Pizotyline	2600	360	25.2%	17.9%	-	-	-	-	-
	Trimipramine	360	180	20.0%	16.4%	-	-	-	-	-
	Doxepin	2100	170	26.1%	18.3%	increased	elongated	n.s.	rescues	rescues
	Nortriptyline	550	200	21.0%	16.5%	-	-	-	-	-
Typical Anti-psychotic phenothiazine (cluster 7)	Acetophenazine	1150	300	17.5%	16.7%	-	-	-	-	-
Cholinergic Antagonist (cluster 7, 8, 9)	Orphenadrine	2250	180	25.5%	14.3%	-	-	-	-	-
	Pridinol	3900	1650	20.6%	15.7%	-	-	-	-	-
	Clidinium	450	420	14.3%	20.5%	-	-	-	-	-
	Procyclidine	850	240	23.3%	18.7%	-	-	-	-	-
	Trihexyphenidyl	3200	170	20.0%	17.8%	-	-	-	-	-

Table S2. Summary table of compounds analyzed. Related to Figures 2-5. *Represents the maximal percent increase of TMRM fluorescence or ATP production relative to in-plate DMSO controls from dose response experiments. Data were generated from 6 independent experiments, with each compound tested in duplicate for each experiment. Significant changes in orthogonal assays are indicated, unless they were non-significant (n.s.) or not measured (-).OCR: oxygen consumption rate.

TRANSPARENT METHODS

Primary neuronal cultures in 384-well microplates for high-throughput screening. Primary neurons were prepared from the forebrains of C57BL/6J or 3xTG (Oddo et al., 2003) mice at P0. Briefly, the brains were dissected in cold buffer (1 x HBSS w/o Ca^{2+} and Mg^{2+}, 25 mM glucose, 20 mM HEPES, 10 mM pyruvate, 2 µg/ml gentamicin) and the meninges removed. Cells were dissociated by incubation with papain (0.015%) for 20m at 37°C followed by 5 cycles of trituration and seeded at $1.5x10^4$ cells/well into black-wall, clear bottom, 384-well poly-D-lysine coated microtiter plates (Greiner) and cultured in Neurobasal medium supplemented with 5% BSA, 2 mM GlutaMAX™ and 2 µg/ml gentamicin. For quality control, we checked the health of the dissociated primary neurons by measuring cell viability using automated cell counter (Invitrogen) according to manufacturer's manual. We only plated primary neurons exceeding 90% viability. The medium was refreshed with Neurobasal A complete medium (1 x Neurobasal A, supplemented with 2% B27, 2 mM GlutaMAX™, 2 µg/ml gentamicin) 4-6h after plating when the cells were firmly attached, and half of the medium was refreshed every 2-3 days until DIV13. Non-neuronal cell division was arrested at DIV4 by the addition of FUdR (8.1 µM 5-Fluoro-2′-deoxyuridine and 20.4 µM Uridine). Plates were covered with Breathe-Easy® sealing membrane (Sigma-Aldrich) to minimize uneven evaporation across each plate in the extended cultures and to permit gas exchange and limit cross-contamination. All experiments were approved by the local IACUC.

Mitochondrial membrane potential ($\Delta\psi_m$) and luminescence-based ATP assays. The assay to measure $\Delta\psi_m$ was performed using the general procedures described in Perry et al. (2011). Changes of $\Delta\psi_m$ in each well were monitored using the mitochondrial-specific, fluorescent dye TMRM (tetramethyl rhodamine, methyl ester; Molecular Probes) and measured using a CLARIOstar plate reader. Our assay development experiments established that 10 nM TMRM provided a non-quenching concentration and a linear assay. This concentration was used throughout our experiments. Compounds known to decrease $\Delta\psi_m$ such as FCCP decreased TMRM fluorescence at 4h or 24h incubation, and were classed as toxic compounds from the screen, while those that increased $\Delta\psi_m$ as shown with increased TMRM fluorescence were identified as potential hits. Neurons cultured to DIV13 in 384-well plates were loaded with 10 nM TMRM for 90m before pin-tooling 100 nl compounds (final concentration, 12.5 µM). After 4 or 24h of incubation, the wells were quickly washed twice with pre-warmed Neurobasal medium to remove free TMRM and the intracellular fluorescence measured by the plate reader (excitation 535 $\pm$ 15 nm, emission 590 $\pm$ 25 nm). Wells in columns 1 and 24 were not loaded with TMRM; these served to measure background signal which was subtracted from the wells to which TMRM was added. To measure the total ATP levels in neurons we utilized the CellTiter-Glo® luminescence-based ATP assay (Promega). DIV13 primary neurons were cultured for 24h with either DMSO carrier or compound treatment, followed by removing 55 µl culture medium from each well. Plates were maintained at room temperature for 25m, and 25 µl of CellTiter-Glo® Reagent with the substrate luciferin was then added to each well (Promega). Plates were covered with aluminum foil and shaken vigorously on an orbital shaker for 10m at 200 rpm and maintained at room temperature for an additional 2m in dark before being read with the plate reader set to the luminescence mode. Dose response experiments were performed by pre-diluting the compounds and pintooling such that DMSO concentration was always kept constant (0.125%).

Compound library and hit picking rules. We screened the 2400 compounds on the MicroSource Spectrum library. This library includes 1600 compounds from the US and International Drug Collections, compounds that have shown biological potential in peer-reviewed publications but have not been developed as drugs, and some nature products derived from

commercial sources. Supplemental Figure 1 provide details of the assays used from which hit picking rules were made. In essence, the average fluorescence for each compound in the TMRM assay was determined and compared to the average fluorescence for compounds in the population on each assay plate to produce a Z-score. The Z-scores for each individual compound assayed across the four replicate plates was then averaged. Because of significant well location effects (outer rows) on each assay plate (Supplemental Figure 1G), we selected primary hits as enhancing well fluorescence above the μ_{plate} by $3\sigma_{plate}$ for inner row wells (rows C-N, columns 3-22), and by $2.5\sigma_{plate}$ for outer row wells (rows A,B, O,P; columns 3-22) (Figure S2C-D). Hits for the orthogonal ATP assay were selected in a similar way as elevating ATP levels by >3 Z-scores compared to within-plate DMSO controls (Figure 1F, Supplemental Figure 1P). All orthogonal assays employed inner wells of the 384-well plates.

Structural clustering. Morgan fingerprints of the rescreened hits were calculated using RDKit. A distance matrix using the dice similarities of the fingerprints was created, and clustering was performed by WPGMA (Weighted Pair Group Method with Arithmetic Mean).

Mitochondrial morphology and neurite area measurements. Mitochondrial morphology and neurite area were quantified using methods described by Varkuti et al, 2020. Briefly, Cre-dependent mitochondrial targeted GFP2 (mito-GFP) ROSA26 knock-in mice were crossed with Ai14 (007908, The Jackson Laboratory) expressing cytosolic-tdTomato, and the forebrain of P0 pups were isolated and primary neurons were cultured as described above. AAV9 virus containing the iCRE sequence driven by the neuron specific CaMKII promoter was added to the cell culture at plating and 75% of the media replaced 4h after plating. Imaging was performed 24 (DIV14) and 48h (DIV15) after compound addition (GE IN Cell Analyzer 6000, 60x objective, 0.95 NA) in confocal mode for mito-GFP (green channel: 3 slices, Δz=0.7 μm, aperture=1.0 AU, λ_{exc}=488 nm, λ_{em}=515-535 nm) and widefield mode for cytosolic-tdTomato (red channel: λ_{exc}=561 nm, λ_{em}=569-641 nm). Z-projected images of the green channel were preprocessed (background subtraction: rolling ball, radius=3; median filtering: radius=1) and somatic mitochondria were removed (see details in Varkuti et al, 2020). Red channel images were also preprocessed (tubeness filter, soma removal). Preprocessed images were segmented by GE Developer software (object-based, kernel size:3). Segmented objects of the green channel were classified as axonal (length: 0.5< Mt_{axon}<=1.4 μm, intensity: >5000, area: >0.25 μm^2, circularity: >0.6) or dendritic (length: >= 2.4 μm, intensity: >5000) mitochondria, while those of the red channel were identified as neurites (intensity > 5000, circularity < 0.5). The length and circularity measurements for mitochondria were aggregated using the median and the area for neurites using the sum. After removing empty fields and outlier values from the fields, aggregated field values were averaged to well values (4 fields/well, 12 wells/compound). Robust Z-scores were calculated using DMSO-treated wells for each well (($median_{compound}$-$median_{DMSO}$)/median absolute $deviation_{DMSO}$), well values were averaged for each compound.

Isolation of brain mitochondria. C57BL/6J mice were randomly selected and grouped to receive either compound (5 mg/kg yohimbine)-supplemented or standard water for 7 months starting at 2 mo of age. The water supply was refreshed weekly. Mitochondria harvested from 2 brains per group were isolated in parallel by differential centrifugation as described by Sims and Anderson (2008), method “A” with some modifications. Briefly, the fresh brain tissue used for respiration experiments was minced and homogenized in a 40 ml Dounce homogenizer with cold isolation buffer (10 mM Tris, 1 mM EGTA, 110 g/L glucose, pH 7.4). All subsequent procedures were performed on ice. The supernatant from two consecutive 5m centrifugations at 1,300 x g were combined and spun for 10m at 21,000 x g. The harvested pellet was resuspended in 15% Percoll and layered above a 23% over 40% Percoll gradient. The gradient was centrifuged at 30,700 x g

for 15m, and the mitochondrial fraction (a band at the 23%/40% Percoll interface) was aspirated. Mitochondria were washed and pelleted at 16,900 x g for 10m, and the loose pellet was precipitated by adding BSA and centrifuging at 6,700 x g for 10m. The final mitochondrial pellet was resuspended in cold MAS-mitochondrial buffer without BSA (70 mM sucrose, 220 mM mannitol, 10 mM KH_2PO_4, 5 mM $MgCl_2$, 2 mM HEPES and 1 mM EGTA, pH = 7.2 adjusted using KOH) and the yield of mitochondrial protein was determined by BCA assay.

Measurement of mitochondrial O_2 consumption. Oxygen consumption rate (OCR) or extracellular acidification rate (ECAR) measurements from permeabilized neurons and isolated brain mitochondria were performed using the XF96 Extracellular Flux analyzer (Seahorse Bioscience). For assays using cultured neurons, primary neurons were dissociated from the forebrains of P0 pups, seeded at $1.9x10^4$/well (PDL-coated XF96 plate), cultured to DIV13 and incubated with selected compounds or DMSO (0.1%) for 24h. Prior to the start of the OCR measurement, all but 30 µl of Neurobasal A/B27 culture medium was removed from each well. Cells were washed twice with pre-warmed MAS-BSA assay medium (70 mM sucrose, 220 mM mannitol, 10 mM KH_2PO_4, 5 mM $MgCl_2$, 2 mM HEPES and 1 mM EGTA, 4 mg/ml fatty-acid free BSA, pH = 7.2 adjusted using KOH) and incubated in 180 ul MAS-BSA medium at 37°C in a CO_2-free incubator for 5m. Following the cartridge calibration, cells were loaded into the XF96 Extracellular Flux analyzer and further equilibrated for 10m with two cycles of 3m mixing and 2m rest prior to the first measurement of basal respiration. OCR and ECAR were measured at 37°C under basal conditions followed by the sequential injection of pre-warmed 10x mitochondrial substrates/ADP (20 µl), oligomycin (22 µl), FCCP (24 µl), and rotenone/antimycin A (26 µl). The final concentrations of injected compounds were as follows: 10mM mitochondrial substrates (pyruvate/malate or succinate), 1 mM ADP, 1.5 µM oligomycin, 3 µM FCCP, 2 µM rotenone/antimycin A. Saponin (25 µg/ml) was co-injected with substrate/ADP to permeabilize the cells and stimulate ADP-dependent respiration. Two baseline measurements were obtained prior to any injection and 2 response measurements were collected after each injection except for after FCCP addition which consisted of 1 measurement (9 total measurements in each assay). Each measurement cycle consists of 2m mixing, 2m waiting, and 3m data acquisition. This protocol allowed for sequential assessment of basal cell respiration, maximal mitochondrial respiratory capacity (State 3 with substrate/ADP), proton leak (State 4_o with oligomycin), uncoupled maximal respiration (State 3_U with FCCP) and non-mitochondrial respiration with the Complex I/Complex III inhibitors, rotenone/antimycin A. Cells were washed twice with MAS buffer to remove residue BSA contained in the assay medium, lysed in 50µl lysis buffer (25mM HEPES, 1mM EGTA, 1mM EDTA, 0.1% SDS, 1% NP-40, 1x protease and phosphatase inhibitor, pH 7.0 adjusted with NaOH) and total protein was determined by BCA assay with a BSA standard curve. Oxygen consumption was normalized to total protein content as pmol O_2/min/ug total protein.

To assay mitochondrial respiration in mice receiving chronic treatment of selected compounds, brain mitochondria were isolated in parallel from C57BL/6J mice receiving water supplemented with or without 25 mg/kg dyclonine or 5 mg/kg yohimbine. The isolated mitochondria were resuspended in MAS buffer without BSA to determine the yield of mitochondrial protein and subsequently further diluted in cold MAS-BSA buffer + substrate (P/M or Succ) to 3 µg/20 ul. This mitochondrial suspension was plated onto PDL-coated 96-well assay plates at 20 µl/well, except for the wells in the four corners which were used for background correction. Note that substrate was initially included and maintained from this step on to help maintain a healthy state of mitochondria. The plate was centrifuged at 2000xg for 20m at 4°C to attach the mitochondria to the XF96 microplates. After centrifugation, 160 µl of MAS-BSA buffer + substrate was added to each well. The mitochondria were checked briefly under the microscope to ensure that the mitochondrial monolayer in each well was homogenous, and then cultured at 37°C in a CO_2-free incubator for 10m. The plates were loaded into the XF96 Extracellular Flux analyzer and further

equilibrated for 8m by two cycles of 1m mixing and 3m rest prior to the measurement of basal respiration. Two baseline measurements were obtained prior to any injection, and one response measurement was obtained after each injection followed by additional 30s mixing. The final concentration of compounds after injections were as follows: 10 mM pyruvate/malate or succinate, 1 mM ADP, 2 μM oligomycin, 4 μM FCCP, 2 μM rotenone/antimycin A. Each measurement cycle consisted of 30s mixing, and 3m data acquisition except for the measurement after ADP injection which lasted 6m. The extension in time for this measurement beyond 3m was included to observe the transition from State 3 to State 4 due to the depletion of ADP in the microchamber. The additional mixing step after each measurement, though optional, facilitated the sensor returning to ambient O_2 concentration. State 3 respiration parameters driven by mitochondrial Complex I substrates (pyruvate/malate) were measured first, while Complex II-driven respiration (succinate) was measured by inhibiting Complex I with rotenone (2 μM).

XF oxygen consumption rate (OCR) was calculated by Seahorse XF96 software package and the algorithm fully described in Gerencser et al. (2009). OCR data measured from isolated brain mitochondria is displayed in the “point-to-point mode” showing a series of OCR rates across each measurement period. OCR data measured from permeabilized neurons is displayed in the “middle point” mode showing a single OCR rate for each measurement period, representing the average of the point-to-point rates.

Data analysis and statistics. All data are presented as mean ± SEM unless otherwise noted. We used the “non-DMSO” control statistic approach for data normalization and hit selection in primary TMRM screen as described in Figure S3. Experimental data containing only two groups were analyzed by Students t-test. A Pearson correlation coefficient was used to probe the relationship between the compounds’ effect-size in TMRM fluorescence and ATP production. Data comparing multiple groups were analyzed by one-way ANOVA followed by Dunnett’s post-hoc test. The data generated by OCR assays were analyzed by two-way repeated measures ANOVA followed by Bonferroni's multiple comparison. The specific tests that were employed and additional information can be found in the legend for each Figure.

Supplemental References

Brideau, C., B. Gunter, B. Pikounis, and A. Liaw. Improved statistical methods for hit selection in high-throughput screening. *J Biomol Screen*. **8,** 634-647 (2003).

Gerencser, A.A., Neilson, A., Choi, S.W., Edman, U., Yadava, N., Oh, R.J., Ferrick, D.A., Nicholls, D.G., and Brand, M.D. (2009). Quantitative microplate-based respirometry with correction for oxygen diffusion. Anal Chem. *81*, 6868-6878.

Malo, N., J.A. Hanley, S. Cerquozzi, J. Pelletier, and R. Nadon. Statistical practice in high-throughput screening data analysis. *Nat Biotechnol*. **24,** 167-175 (2006).

Oddo, S., Caccamo, A., Shepherd, J.D., Murphy, M.P., Golde, T.E., Kayed, R., Metherate, R., Mattson, M.P., Akbari, Y., and LaFerla,. FM. (2003). Triple-transgenic model of Alzheimer’s disease with plaques and tangles: intracellular Abeta and synaptic dysfunction. Neuron *39*, 409-421.

Perry, S.W., Norman, J.P., Barbieri, J., Brown, E.B., and Gelbard, H.A. (2011). Mitochondrial membrane potential probes and the proton gradient: a practical usage guide. Biotechniques. *50*, 98-115.

Sims, N.R., and Anderson, M.F. (2008). Isolation of mitochondria from rat brain using Percoll density gradient centrifugation. Nat Protoc. *3*, 1228-1239.

Varkuti, B.H., Kepiro, M, Liu, Z., Vick, K., Avchalumov, Y., Pacifico, R., McMullen, C.M., Kamenecka, T.M., Puthanveettil, S.V., and Davis, R.L. (2020). Neuron-based high-content assay and screen for CNS active mitotherapeutics. Science Advances *6*, eaaw8702.